STUDIES INTO THE MECHANISM OF A PHOTOCHEMICAL HYDROGEN ABSTRACTION REACTION AND A PHOTOVOLTAIC EFFECT

by

MICHAEL H. ZUDIKER

A dissertation submitted to the Graduate Faculty in Chemistry in partial fulfillment of the requirements for the degree of Doctor of Philosophy, The City University of New York.

1975

This manuscript has been read and accepted for the Graduate Faculty in Chemistry in satisfaction of the dissertation requirement for the degree of Doctor of Philosophy.

April 25, 1975
date

Adam Heller
Chairman of Examining Committee

April 29, 1975
date

Leonard H. Schwartz
Executive Officer

Norman L. Goldman
Robert Bittman
Supervisory Committee

The City University of New York

Abstract

STUDIES INTO THE MECHANISM OF A PHOTOCHEMICAL HYDROGEN ABSTRACTION REACTION AND A PHOTOVOLTAIC EFFECT

by

Michael H. Zudiker

Adviser: Professor Adam Heller

The isotope effect in the photochemical hydrogen abstraction reaction of benzophenone with benzhydrol is shown to have at least some temperature dependence between 8° and 58°C. Although this dependence may be due to factors inherent only within this system, it may also be due to differences in zero point energies. It is, therefore, not possible to determine the extent to which this effect is controlled by differences in vibrational frequencies.

The photovoltaic effect exhibited by potassium octacyanomolybdate is shown to be due to a hydrolysis rather than an electron photoejection reaction. Polarographic studies show that two intermediates are produced simultaneously during initial irradiation. It is postulated that these are isomeric forms of $Mo(CN)_7^{-3}$. Although limited by its speed of response, poloragraphy is shown to be a useful tool in distinguishing intermediates with similar absorption spectra.

Acknowledgements

I first wish to thank the Chemistry Faculty of Queens College and all the people in the exploratory research group of GTE Laboratories without whose help I would not have overcome the research barriers in my path. I would separately like to thank Seth Grenetz and Dan Casella for their firm friendships during this period. I leave for last the most important person. Without the extreme patience and encouragement of my wife, Mona, none of this would have been possible.

TABLE OF CONTENTS

PART I. TEMPERATURE STUDY OF A PHOTOCHEMICAL ISOTOPE EFFECT

Chapter Page

LIST OF TABLES

LIST OF FIGURES

PART I

PART II

PART I

TEMPERATURE STUDY OF A PHOTOCHEMICAL ISOTOPE EFFECT

CHAPTER I

INTRODUCTION

Theories of Radiationless Transitions Related to Isotope Effects

Introduction

Deuteration of organic molecules in certain systems increases the lifetime of excited states. Upon deuteration, the phosphorescent lifetime of naphthalene increases from 2.3 seconds to 22.0 seconds[1]; benzene from 7.0 seconds to 26.0 seconds[2]. Deuteration also decreases the rate of photochemical reduction reactions, producing a primary isotope effect. Moore & Ketchum[3] found an isotope effect of 2.7 in the photoreduction of benzophenone by benzhydrol and benzhydrol-d_1. Coulson and Yang[4] found the triplet lifetime of 2-hexanone to increase 2.3 times with substitution of one deuterium at the 5 position, 7.0 times with two deuteriums at this position. Yang[5] found an isotope effect of 2.8 from 25° to 202°C for the quenching of Hg ($^3P_1$) by C_3H_8 and $CH_3CD_2CH_3$.

The various theories of radiationless decay of excited states give an explanation of these phenomena. At the same time the results predicted by these theories have yet to be tested.

Radiationless decay occurs as a result of transitions

from one excited state in a molecule to another or from the transfer of electronic energy from one molecule to another, without the emission of light.

Robinson and Frosch Theory[6]

Robinson and Frosch considered the coupling of a nonstationary initial state, Ψ', and a degenerate final state, Ψ''. The initial state is in its lowest vibrational level. The final state is made degenerate with the initial state by the inclusion of the vibrational energy levels. For example, the initial state can be an excited singlet with the final state being a triplet. The triplet is made isoenergetic with the singlet by addition of higher vibrational levels. The perturbation, H', arises from coulombic interactions of the electrons and nuclei of the system. The energy of coupling, β_n, between the initial state and the final state can be determined by the following relationship:

(1) $$\beta_n = \langle \Psi' | H' | \Psi'' \rangle$$

The Born-Oppenheimer approximation considers the interaction between electronic and nuclear motion to be independent. In effect, these motions can be considered two mutually independent oscillators, one of high frequency, one of low. Using this approximation β_n can be divided into two parts. One consists of the electronic interaction β_{el}, the other the nuclear interaction,

(2) $$\beta_n = \beta_{el} \langle \Phi_n'' | \Phi' \rangle$$

The integral, $\langle \Phi_n'' | \Phi' \rangle$, is the vibrational Franck-Condon overlap integral. It measures the degree of overlap between the vibrational eigenfunctions of two electronic states. Figure 1 shows the vibrational overlap between the lowest excited singlet at the J = 0 level, a triplet state and the ground state. For efficient energy transfer to occur the J = 3 vibrational level of the triplet and the J = 10 state of the ground state must be considered. Since oscillations around the energy level increase as J increases, the net result is zero overlap with the ground state and at least some overlap from the triplet state.

The radiationless transition per unit time, w(t)/t, is given by equation 3 where α is the energy of indirect coupling between the two states and all other states including the solvent.

(3) $$\frac{w(t)}{t} = \frac{2\pi\beta_{el}}{\alpha\hbar} \Sigma \langle \Phi n'' | \Phi' \rangle^2$$

Siebrand Theory[7]

Siebrand considered the Franck-Condon factors associated with the Robinson-Frosch Theory. An empirical relationship was presented for the rate of radiationless transitions from an excited triplet to ground state singlet for an aromatic hydrocarbon:

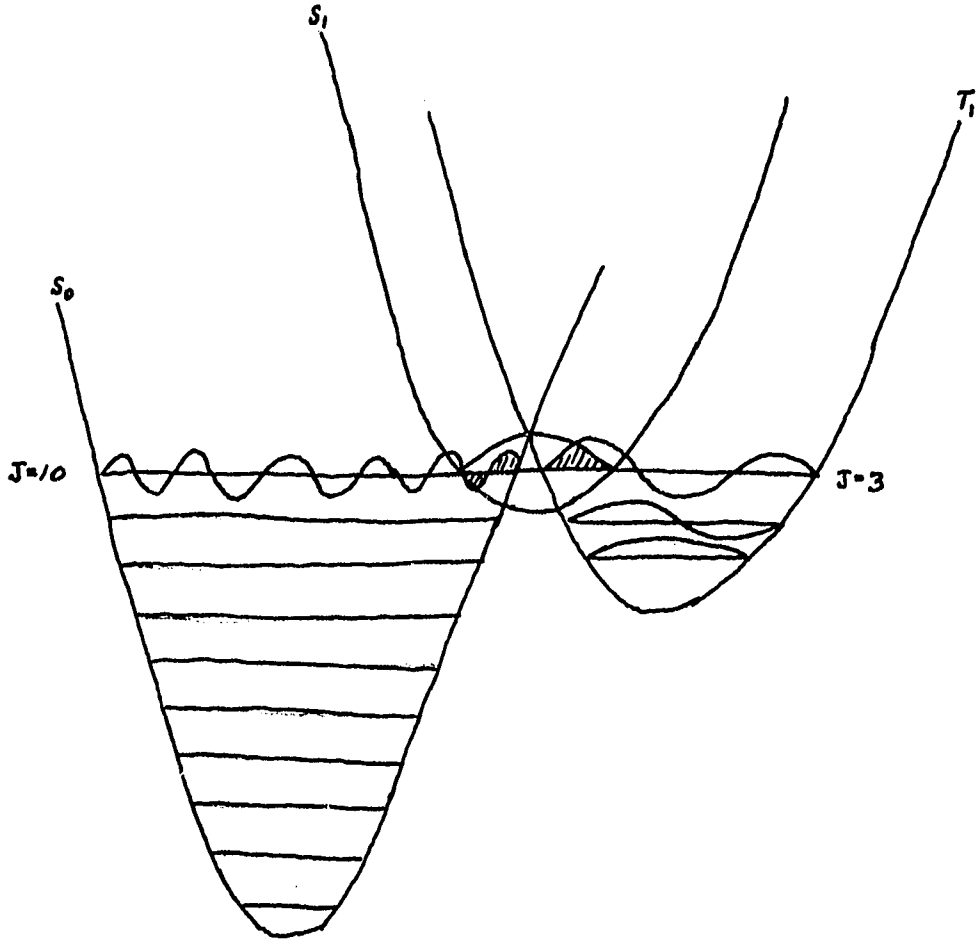

Fig. 1.--Franck-Condon Vibrational Overlap

(4) $\text{Log } K = \text{Log } K_o - f\ (E-E_o/n)$

where K_o is the radiationless rate constant for all aromatic hydrocarbons, K is the radiationless rate constant for $T_1 \rightarrow S_o$, E is the difference in energy levels, E_o is $4000cm^{-1}$ for an aromatic C-H bond and $5500cm^{-1}$ for an aromatic C-D bond, and $n = N_H/N_H+N_C$, where N_i is the number of atoms of type i in the molecule. In order for reasonable correlation with experimental data, corrections had to be made in this relationship. These included the inclusion of the stretching frequency of either the C-H or C-D bonds and the consideration that these vibrations are anharmonic rather than harmonic oscillators.

Other Theories

Lin[8] extended Robinson's theory by including a Boltzman distribution of initial vibronic states rather than just the lowest vibrational level. Kasha[9] and Jortner[10] independently considered that radiationless transitions are caused by a breakdown in the Born-Oppenheimer approximation for vibronic states similar in energy.

Recent workers have considered radiationless transitions in an isolated molecule with no interaction from the environment. Henry and Siebrand[11] considered the perturbation to be spin-orbit coupling as well as nuclear momentum. Three classes of radiationless transitions can then be considered. The first is radiationless transitions

due to spin-orbit coupling. The second is due to spin-orbit plus vibronic coupling and the third is due to spin-orbit and non Born-Oppenheimer coupling. In all three cases, the Frank-Condon overlap integrals can be factored out, but in the second and third cases, vibrational frequency factors are also included in the electronic wavefunction. This leads to the conclusion that stretching and bending vibrations are responsible for both the promotion and acceptance of energy. Deuteration affects the rate of transitions by decreasing the extent of vibronic coupling. The position of the deuterium on the molecule will, therefore, affect the degree of coupling and the nonradiative lifetime. However, in the case of aromatic carbon compounds, whose lowest state is $\pi\pi^*$, the decreased rate of radiationless transitions upon deuteration results primarily from decreased Franck-Condon overlap[12].

Benzene Studies--Isolated Molecule[13-19]

The most studied isolated molecule has been benzene vapor at low pressure. Rates of radiationless and radiative transitions have been measured from as many as twenty-two individual vibronic states in the molecule and it has been found that rates of intersystem crossing increase as the excess vibrational energy in the excited state is increased[13-19]. Spears and Rice[13] have shown that low frequency out of plane vibrational modes have

shorter nonradiative lifetimes than symmetric vibrations. They also found certain vibronic states in which direct photochemical reaction seemed to occur. Heller, Freed, and Gelbart[19] studied the rates of nonradiative transitions in a vibronic level relative to the rates of the lowest vibronic level of that mode. They found that for systems in which the energy separation is large between the lowest singlet and triplet and vibronic coupling is weak:

1. As the excess excitation energy increases, C-C modes become more efficient in competing for the energy.

2. With C-D modes present, C-C modes become more efficient in competing for the energy.

3. When the frequency difference ($\delta\nu = \nu^t - \nu^S$) between acceptor and donor modes is positive. The relative rate will increase with increasing excess energy. The opposite is true of $\delta\nu<0$.

4. For acceptor modes, the most efficient are those that contain geometric or frequency changes and maximum vibrational frequencies. In benzene the C-H modes have both a geometric change and large vibrational frequency.

Other Explanations[20-24]

Certain effects occur on deuteration that cannot be explained by the general theories of radiationless transitions. Johnson and Ziegler[20] found that the isotope effect on the triplet lifetime of benzene in an argon matrix at

20°K is due to the effect C-D vibrations have on radiative rather than nonradiative transitions. Gelbart, Freed, and Rice[21] explain the nonexistence of an isotope effect on the isomerization of stilbenes as the result of energy transfer to torsional rather than vibrational modes. The inverse isotope effect on the lifetimes of some aromatic hydrocarbons has been explained by Scharf and Silbey[22] as the result of the coupling of the excited singlet with a higher triplet state. Fischer[23] ascribed the same phenomenon to a crossing of a hypersurface with the lowest triplet. The inverse effect would then be due to differences in zero point energy of the C-H and C-D bonds causing a greater overlap for C-D vibrations. The latter theory explains the temperature dependence of the isotope effect for anthracene from 77°K-420°K found by Lin and Bhattacharjee[24] but does not explain the magnitude of the effect.

Heller Theory[25]

Heller extended these theories qualitatively to include photochemical hydrogen abstraction reactions. His proposed model was summarized in four rules.

1. "The lower the dissociation energy of the reactive bond or the larger the anharmonicity of the stretching vibration association with it, the higher the photochemical reactivity." The anharmonicity factor increases the overlap of the vibrational functions. In addition, it permits

vibrational transitions greater than $\delta v \pm 1$ to occur.

2. "The lower the density of hydrogen atoms in the environment of the reactive system, the higher the photochemical quantum yield." The greater the number of vibrational modes the greater will be the competition from these modes for the electronic energy.

3. "The closer the center of electronic excitation and the reactive bond, the higher the photochemical activity." The interaction decreases with the sixth power of the distance between donor and acceptor.

4. "The most reactive bonds are those that have high vibrational frequencies." Since radiationless relaxation depends on the overlap of vibrational orbitals, the higher the vibrational frequency of the acceptor, the lower the vibrational orbital needed to accept the energy and the greater the possible overlap with the donor vibrational level. A C-D bond will be less reactive than a C-H bond since its vibrational frequency is 0.7 times smaller.

5. Since these overlap integrals are not temperature dependent, an isotope effect, k_H/k_D for an abstraction reaction would be temperature independent.

Zero Point Energy Isotope Effect-Theory

Introduction[26]

An isotope effect can also be caused by the difference in zero point energies between carbon-hydrogen and carbon-deuterium vibrations rather than by the difference in their vibrational frequency. The zero point energy is related to the frequency of vibration with the latter being dependent on the masses of the atoms and on the force constant between the atoms.

The vibrational frequency is determined by the following relationship

$$(5) \qquad \nu = \frac{1}{2\pi c} (k/\mu)^{1/2}$$

where c is the speed of light, k is the force constant and μ is the reduced mass (approximately equal to 1 for hydrogen and 2 for deuterium).

$$(6) \qquad \nu_H/\nu_D = (M_D/M_H)^{1/2} = 1.4$$

Since the zero point energy is equal to $1/2h\nu$ the zero point energy for C-H will be 1.15 Kcal higher in energy than for C-D.

First Approximation[26]

In the first approximation, it is assumed that only the C-H bond will be broken during reaction, resulting in an activated complex containing no zero point energy

difference. Consequently, there would be a larger activation energy and a slower rate of reaction for a C-D bond as compared to a C-H. The ratio of the rates of reaction is given by equation 7 while Table 1 shows the changes in isotope effect values for a C-H vibration from 0° to 500° using this equation.

$$(7) \qquad k_H/k_D = e^{h(\nu_H-\nu_D)/2kT}$$

Absolute Rate Theory[27]

A more refined explanation of the isotope effect can be found by use of absolute rate theory. Equation 8 gives the expression for the absolute rate of the reaction where the expression in brackets accounts for tunneling effects,

$$A+B \ldots \rightarrow M^{\ddagger}+N$$

$$(8) \qquad \text{Rate} = [1-\frac{1}{24}(\frac{h\nu_L{}^{\ddagger}}{kT})^2]\kappa\frac{kT}{h}K^{\ddagger}\frac{[A][B]\cdots}{[N]\cdots}\cdot\frac{\alpha_A\alpha_B\cdots}{\alpha^{\ddagger}\alpha_N\cdots}$$

κ is the transmission coefficient or the fraction of efficient transitions across the barrier, $\nu_L{}^{\ddagger}$ is the vibrational frequency across the reaction pathway, α is the activity coefficient, and $K^{\ddagger}$ is an equilibrium constant, equal to the ratio of the partition function of the transition state, $Q^{\circ\ddagger}$, to that of the reactants, Q° (Equation 9).

$$(9) \qquad K^{\ddagger} = Q^{\circ\ddagger}/Q^{\circ}$$

The partition function, $Q^{\circ\ddagger}$ and Q°, consist of the product of partion functions for translational, rotational,

TABLE 1[26]

ISOTOPE EFFECT VALUES FOR C-H VIBRATIONS

$h\nu_H - h\nu_D$	T°C	k_H/k_D
1150	0	8.3
	25	6.9
	100	4.7
	200	3.4
	300	2.7
	500	2.1

and vibrational motion. These three functions are given in equations 10, 11, and 12 respectively, where h, k, and T have their usual meaning, M is the molecular mass, A, B, and C are the moments of intertia , and ν_i is the frequency of vibration.

$$(10) \qquad Q_{trans} = \frac{(2\pi MkT)^{3/2}}{h^3}$$

$$(11) \qquad Q_{rot} = \frac{8\pi^2(8\pi^3 ABC^{1/2}(kT)^{3/2}}{h^3}$$

$$(12) \qquad Q_{vib} = \prod_i e^{-1/2h\nu_i/kT}(1-e^{-h\nu_i/kT})^{-1}$$

In determining the extent of an isotope effect, it is first assumed that differences in tunneling, activity coefficient, and transmission coefficient between isotopic species are negligible. This results in the isotope effect being determined by the ratio of equilibrium constants for the two isotopic species; consequently k_H/k_D can be determined by a ratio of partition functions.

$$(13) \qquad k_H/k_D = k^{\ddagger}_H/k^{\ddagger}_D = Q^{\circ\ddagger}_H/Q^{\circ\ddagger}_D \times Q^{\circ}_D/Q^{\circ}_H$$

The next assumption made is that the bond cleaved is that stretching vibrational mode which corresponds to the aperiodic motion along the reaction coordinate. This vibrational energy is converted to translational energy. This results in the activated complex having one less vibrational mode than the reactants. The resulting expression for the isotope effect is given in equation 14, where

μ has replaced $h\nu/kT$, n is the number of atoms in the

$$(14) \qquad k_H/k_D = \left(\frac{M_H^{\ddagger}}{M_D^{\ddagger}} \times \frac{M_D}{M_H}\right)^{3/2} \left(\frac{A_H^{\ddagger}B_H^{\ddagger}C_H^{\ddagger}}{A_D^{\ddagger}B_D^{\ddagger}C_D^{\ddagger}} \times \frac{A_DB_DC_D}{A_HB_HC_H}\right) X$$

$$X \prod^{3n-7} \frac{1-e^{-\mu_H}}{1-e^{-\mu_D}} \prod^{3n-6} \frac{1-e^{-\mu_H}}{1-e^{-\mu_D}} X$$

$$X \exp\left\{-1/2\left[\sum^{3n^{\ddagger}-7}(\mu_H^{\ddagger}-\mu_D^{\ddagger}) - \sum^{3n-6}(\mu_H-\mu_D)\right]\right\}$$

ground state and $n^{\ddagger}$ is the number in the excited state.

Several assumptions are then made. The first of these is that differences in molecular mass and moments of inertia between ground and transition state or between different isotopic species is negligible and, therefore, the first two factors in equation 14 are approximately equal to one. Then, since the factor $e^{-\mu}$ is negligibly small compared to one, the same can be assumed for the first segment of vibrational factors. This leaves the remaining vibrational factor as the cause of the isotope effect.

$$(15) \qquad k_H/k_D = \exp\left\{-1/2\left[\sum^{3n^{\ddagger}-7}(\mu_H^{\ddagger}-\mu_D^{\ddagger}) - \sum^{3n-6}(\mu_H-\mu_D)\right]\right\}$$

The interesting point of this expression is that it relates the isotope effect to differences in zero point energy in both the ground and transition state. At no point is the activation energy considered.

It is is now assumed that the interaction between the decomposing molecule and all other molecules is weak so that the transition state contains no three-centered complex, the values of n and $n^{\ddagger}$ are equal, and all vibrational factors will cancel except for the extra vibrational mode found in the ground state. The resulting expression for the isotope effect is the exact equivalent of that given in equation 7.

$$(16) \qquad k_H/k_D = \exp\{1/2[\frac{h\nu_H}{kT} - \frac{h\nu_D}{kT}]\}$$

Three Centered Transition State

It should be stated at this point that the isotope effect values calculated by use of equation 16 and shown in Table 1 are the result of a great number of assumptions and approximations and can only be looked upon as being the maximum obtainable value. Although many reactions exhibit isotope effects which approach these values, many other reactions have isotope effects far below them. A probably reason for these discrepancies is the assumption of a two-centered transition state with no effect from other reacting molecules. This is certainly not the case in many hydrogen abstraction and SN2 reactions.

In the two-centered approximation, the molecule contained one linear vibration, an aperiodic mode along the reaction coordinate. This vibration was lost in the

transition state with a resulting isotope effect. Using the three-centered approach there are two possible linear modes. One of these modes will be lost in the transition state while the remaining mode may or may not have a zero point energy difference. If the two heavy atoms, X and Y, are the same, the aperiodic motion along the reaction coordinate corresponds to the mode shown in Figure 2a. The periodic motion which remains corresponds to that in Figure 2b in which there is little or no vibration of the central atom relative to X and Y. Substitution of deuterium for hydrogen will result in no zero point energy difference in the transition state and a normal isotope effect. If, however, X and Y are different atoms or if their force constants with hydrogen are different, the central atom will exhibit some vibration. This will have the effect of producing a zero point energy difference in the transition state and decreasing the isotope effect. The extent of the decrease in isotope effect will depend on the degree of vibration of the central atom.

As stated earlier, an isotope effect due to difference in vibrational frequency will be temperature independent since the Franck-Condon overlap integral are not temperature dependent. However, an isotope effect due to difference in zero point energy would have a temperature dependence determined by equation 16.

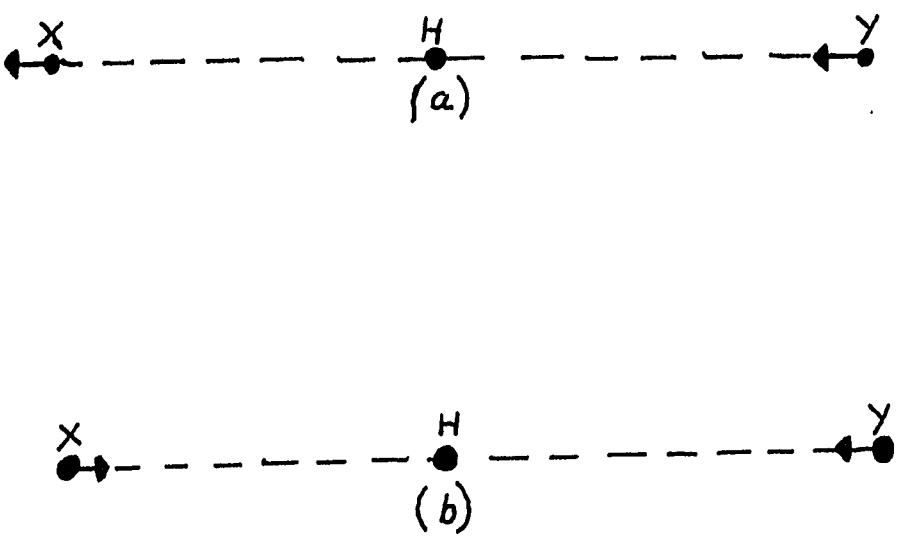

Fig. 2.--Normal vibrational modes for a three-centered transition state.

The System Studied--Ketone Photoreduction

Introduction

In order to test Heller's proposal that the isotope effect arising from a difference in the vibrational energy of a C-H compared to C-D bond in a photochemical reduction reaction is temperature independent, a system was selected that had been well studied and in which the photochemical and photophysical pathways were understood.

Ketone photoreduction is such a reaction. The carbonyl group upon excitation with light abstracts a hydrogen atom from an appropriate source to form a hydroxy group and a carbonyl radical. The reaction can occur with diaryl ketones[29-32], aryl-alkyl ketones[29-31,33], and dialkyl ketones[29, 31, 34-36] and can be intramolecular if a γ hydrogen is present in the molecule[37-41]. The reactive excited state can be either a singlet or triplet[31,32,37], but must be a $n\pi^*$ in nature[42-52]. The proton source can be an alcohol[30,53,55,94], hydrocarbon[54,55], amine[56-58], ether[59], or aromatic[60,61].

Benzophenone--Photophysical Studies

The most studied case of ketone photoreduction is that of benzophenone[42,50,53,59]. The energies of the lowest excited states of benzophenone have been measured by many techniques including singlet-singlet absorption, singlet-triplet absorption, phosphorescence lifetimes, and

phosphorescence excitation. Table 2 shows the energies determined for the lowest excited singlet and triplet for this molecule. The singlet energy is between 26,000 cm^{-1} and 27,300 cm^{-1} and the triplet energy is between 24,000 cm^{-1} and 24,800 cm^{-1} depending on the medium. The singlet-triplet energy difference is therefore about 2,000 cm^{-1}.

The singlet state does not exhibit appreciable fluorescence[70], $\phi_f = 10^{-5}$, but has been determined to be an $n\pi^*$ transition by its absorption shifts with various polar and nonpolar solvents, its vibrational fine structure, its low extinction coefficient, and its similarity to $n\pi^*$ absorption in similar compounds[50]. The low fluorescence yield has been shown to be due to efficient intersystem crossing from singlet to triplet[71-74]. A low yield of delayed fluorescence has been found in carbon tetrachloride solution at 298°K[75].

The triplet state is known to be $n\pi^*$ character by its short lifetime, vibrational fine structure, solvent effects, and lack of phosphorescence enhancement with the addition of heavy atoms[42,43,68]. Phosphorescence is exhibited in the crystalline state, in glass matrices and in certain solutions such as perfluoremethylcyclohexane, benzene, carbon tetrachloride, and isooctane at room temperature. The lifetime has been determined by phosphorescence

TABLE 2

ENERGIES OF THE FIRST EXCITED SINGLET AND TRIPLET STATES OF BENZOPHENONE

Energy of Singlet	Energy of Triplet	Solvent	Method	Reference
	24,400	Liquid Paraffin	T-T	62
26,400	24,265	Hexane	S-S T-T	63
26,500		Crystal	S-S	
	24,185	EPA	phos.	
26,000	24,200	EA*	phos.	64
	23,860	Pet. Ether	phos.	65
	24,300	EPA	phos.	66
	23,800	Crystal	phos.	
	24,195	Crystal	phos.	67
27,300		EPA	S-T	42
27,027		MC**	S-T	
	24,213	EPA	phos.	
	23,981	MC	phos.	
	24,814	EPA	S-T	

*Ethanol + Diethyl ether glass

**Methylcyclohexane glass

TABLE 2--Continued

Energy of Singlet	Energy of Triplet	Solvent	Method	Reference
27,000		EPA	S-S	50
	24,250	EPA	phos	
27,000	24,800	EET***	S-S S-T	68
	24,210	EPA	phos.	69
	24,660	PMMA****	phos.	
	23,980	PE*****	phos.	
	24,070	Crystal	phos.	
	23,890	MC**	phos.	

**Methylcyclohexane glass

***Ethanol, Ether, Toluene glass

****Polymethylmethacrylate

*****Polyethylene

decay, singlet-triplet absorption, and energy transfer studies. Table 3 shows that the value of τ, the triplet state lifetime, determined below 108°K is between 4×10^{-3} and 6×10^{-3} sec.

In liquids, above 108°K, the lifetime of the triplet is considerably shorter (Table 4). The two-fold, ten-fold, or even greater difference in lifetimes under the two conditions may result from impurity quenching, self quenching[77], specific interaction with the solvent[43,60,76,78], quenching by radicals formed by hydrogen abstraction from the solvent or quenching by secondary products formed from the abstraction reaction[61,75,79,82].

Benzophenone--Photochemical Studies

The following mechanism for the photoreduction of benzophenone by benzhydrol was originally proposed by Moore, Hammond and Foss[83], and expanded by Moore and Ketchum[3] to include the effect of added quenchers.

$$(C_6H_5)_2CO \xrightarrow{h\nu} (C_6H_5)_2CO^* \qquad aI$$

$$(C_6H_5)_2CO^* + (C_6H_5)_2CHOH \rightarrow 2(C_6H_5)_2\dot{C}\text{-}OH \qquad k_H$$

$$(C_6H_5)_2CO^* \rightarrow (C_6H_5)_2CO \qquad k_d$$

$$Q + (C_6H_5)_2CO^* \rightarrow (C_6H_5)_2CO + Q \qquad k_q$$

$$2\ (C_6H_5)C\text{-}OH \rightarrow [(C_6H_5)_2\dot{C}\text{-}OH]_2 \qquad k_c$$

TABLE 3

LIFETIME DETERMINATIONS OF THE TRIPLET STATE OF BENZOPHENONE BELOW 108°K

Lifetime (msec)	Temperature (°K)	Solvent	Method	Reference
1	77-108	Isopentane	S-T	43
6	77	EPA	phos.	42
6	20	Crystal	phos.	71
6	77	Crystal	phos.	76
4.7	77	EPA	phos.	50
4	77	EET	S-T	52
4.7	77	EA	phos.	64
5.8	77	EPA	phos.	60
5	77	PMMA	phos.	69
4.9	77	MC	phos.	
3.7	77	Crystal	phos.	

TABLE 4

LIFETIME DETERMINATIONS OF THE TRIPLET STATE OF BENZOPHENONE ABOVE 108°K

Lifetime (msec)	Temperature (°K)	Solvent	Method	Reference
$\geq 10^{-3}$	108-298	Isopentane	S-T	43
6.5×10^{-3}	298	Benzene	phos.	76
2.5×10^{-3}	298	Isoctane	phos.	
1×10^{-2}	298	Benzene	S-T	84
1.9×10^{-3}	293	Benzene	Energy Transfer	88
4.0×10^{-2}	298	PFM*	phos.	77
2.0×10^{-2}	298	TTE**	S-T	85
1.2×10^{-2}	298	Benzene	S-T	60
8.4×10^{-3}	296	Benzene	phos.	75
1.1×10^{-1}	296	Carbon Tetra-chloride	phos.	

*Perfluormethylcyclohexane

**1,1,2 Trifluor-Trichloroethane

Here a is the yield of chemically active excited state, I is the intensity of light, k_H is the rate of hydrogen abstraction, k_d is the rate of radiationless deactivations, including all pseudounimolecular deactivations and k_q is the rate of quenching.

Since the lifetime of the singlet state is short and intersystem crossing to the triplet is efficient, a = 1, and the reactive excited state is the $n\pi^*$ triplet. Further evidence for this is the decrease in the lifetime of the triplet state and the corresponding increase in ketyl radical concentration when a proton source is added. Furthermore, triplet quenchers efficiently decrease the concentration of ketyl radical[43,60,84-87].

With the assumption that the concentration of triplet assumes a steady state, the quantum yield for the disappearance of benzophenone, ϕ, is equal to

$$1/\phi = 1 + \frac{k_d + k_q(Q)}{k_H[(C_6H_5)_2CHOH]} \qquad (17)$$

Plots of $1/\phi$ vs [Q] give the value of k_q/k_H, while plots of $1/\phi$ vs $1/(C_6H_5)CHOH$ in the absence of triplet quenchers give the value of k_d/k_H. The best values for k_q/k_H and k_d/k_H are 750[89,51] and $0.033 M^{-1}$ respectively[90]. For quenchers like naphthalene, the rate of quenching is diffusion controlled so that k_q is equal to 5×10^9 M^{-1} sec^{-1}[79]. The value of K_H is then calculated to be $7 \times 10^6 M^{-1} sec^{-1}$ and

k_d is equal to $2x10^5 sec^{-1}$. The value of k_d is in agreement with values determined by physical methods (Table 4).

The reaction can be quenched by methods other than physical quenching. Mercaptans and disulfides quench by reaction with the ketyl radical to reform benzophenone[38,91].

$$\phi_2\dot{C}\text{-OH} + RS\cdot(RSSR) \rightarrow \phi_2C = O + RSH(RSH + RS\cdot)$$

Amines, such as diphenylamine and triethylamine, efficiently quench the photoreduction by a primary reduction of the benzopheonone triplet[56-58a,92,93].

$$\phi_2C{=}O^{3*} + \phi_2NH \rightarrow [\phi_2\dot{C}O^- \cdots \phi_2\overset{+\cdot}{N}H] \begin{cases} \rightarrow \phi_2C{=}O + \phi_2NH \\ \rightarrow \text{Products} \end{cases}$$

The quenching is enhanced by electron-donating substituents and decreased by electron-withdrawing groups. Although the quenching efficiency seems to be correlated with the ease of electron loss, there are still anomalies present.

By using deuterium rather than hydrogen in the tertiary position of benzhydrol, an isotope effect, k_H/k_d, was found to be 2.7[83]. This gives the rate of deuterium abstraction to be $2.6x10^6\ M^{-1}sec^{-1}$.

This part of the dissertation centers on the measurement of the temperature dependency of the isotope effect of benzophenone in the presence of benzhydrol and benzhydrol-d_1.

CHAPTER II

EXPERIMENTAL

Chemicals

Benzophenone: Fisher, certified grade, recrystallized twice from ethanol.

Naphthalene: Fisher, certified grade, recrystallized twice from ethanol.

Benzene: Matheson Coleman and Bell (MCB) chromatoquality.

Benzhydrol: Fisher highest purity, recrystallized once with ligroin, twice with MCB chromatoquality cyclohexane, and twice from MCB spectroquality 1,1,2-trichlorotrifluoroethane.

Benzhydrol-d_1: The compound was synthesized by a known procedure[95] with the modification that twice the calculated amount of $LiAlD_4$ was used to insure completeness of reaction. To 0.1 mole $LiAlD_4$ in 200 ml absolute ether, 0.2 mole benzophenone dissolved in absolute ether was added over a period of 2 hours. After the addition was completed, the reaction mixture was set to reflux for an additional hour. The reaction was cooled and 50 ml of water was added slowly with stirring. A solid precipitate of $Al(OH)_3$ and LiOH formed. The solution was decanted, into a

separatory funnel and 125 ml of a 10% H_2SO_4 solution was added. The ether layer was separated, dried over $MgSO_4$ and evaporated until approximately 100 ml remained. The remaining solvent was evaporated over nitrogen. The white solid remaining was recrystallized twice from spectroquality 1,1,2-trichlorotrifluoroethane. The melting point of the white crystalline product was 64.5-65.0°. The yield was 22 grams. The IR spectrum of benzhydrol and benzhydrol-d, were identical except for the absence of the C-H peak at 2870 cm^{-1} and the presence of the C-D peak at 2140 cm^{-1} for benzhydrol-d_1 (Figure 3). Analysis: Calculated Carbon 84.7%, Hydrogen 6.53%: Observed-Carbon 85.4%, Hydrogen 6.23%.

Degassing Procedure

The reaction cells were fabricated from optically flat quartz tubing obtained from the Opticell Company having a 1-cm path length and an extension tube leading to a teflon greaseless vacuum stopcock and followed by an O-ring glass joint for connection to a vacuum line (Figure 4). This allowed irradiation and absorption measurements to be made without removal of material undergoing reaction.

Degassing was performed using a greaseless and mercury-free oil diffusion vacuum system. Stopcocks were made of teflon and pressure measurements were made with both a

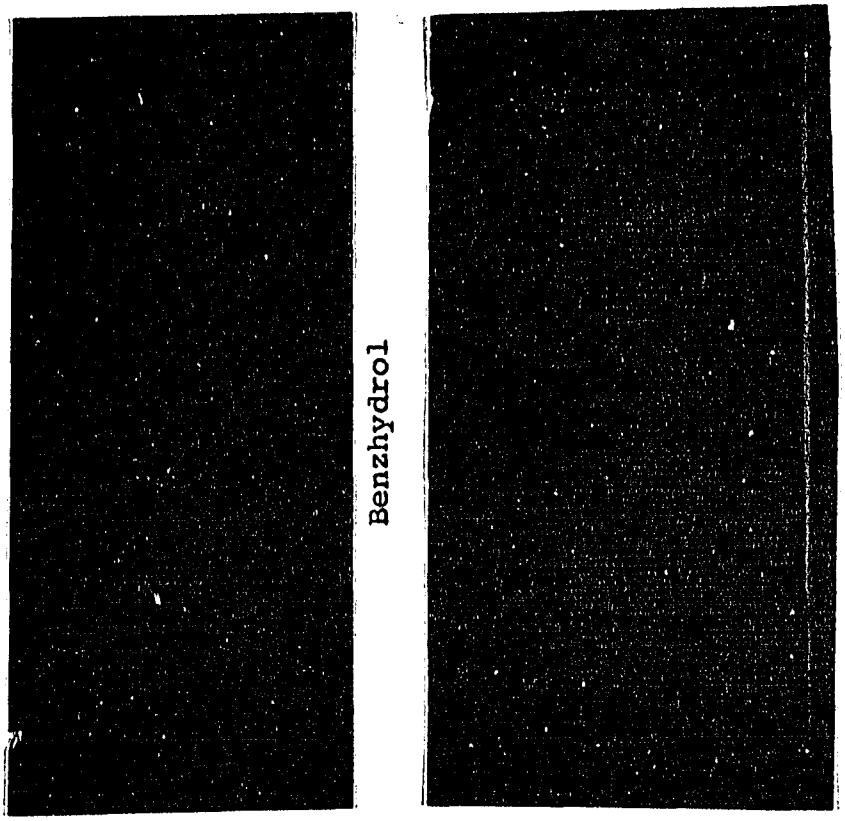

Fig. 3.--IR Spectra of Benzhydrol and Benzhydrol-d_1

thermocouple and Pirani ionization gauge. All joints were O-ring glass joints. The solution to be degassed was poured into the bottom of a cold finger, fitted on the top with two reaction cells (Figure 5). The cold finger plus cells were connected to the vacuum system. The solution was zone frozen using liquid nitrogen open to the vacuum system and evacuated to 10^{-5} torr. The cold finger was then closed off from the vacuum system, the solution was allowed to thaw, was frozen again and opened to the system. After seven of these freeze-thaw cycles had been completed, an overpressure of argon was allowed into the system. The cold finger was closed off from the vacuum line, detached, and rotated two times to fill the cells with the degassed solution; the cell stopcocks were then closed and disengaged from the cold finger. The cells were stored in the dark for use within twenty-four hours.

Irradiation Procedure

Irradiation was performed using a Hanovia 1,000-watt Xe-Hg high-pressure lamp. A typical, relative emission spectrum is shown on Figure 6. Specifications for the lamp are given in Table 5.

The optical system consisted of a saturated $CuSO_4$ infrared filter, a convex lens (focal length 32 mm) to form a point source of light and a convex lens (100 mm) used to

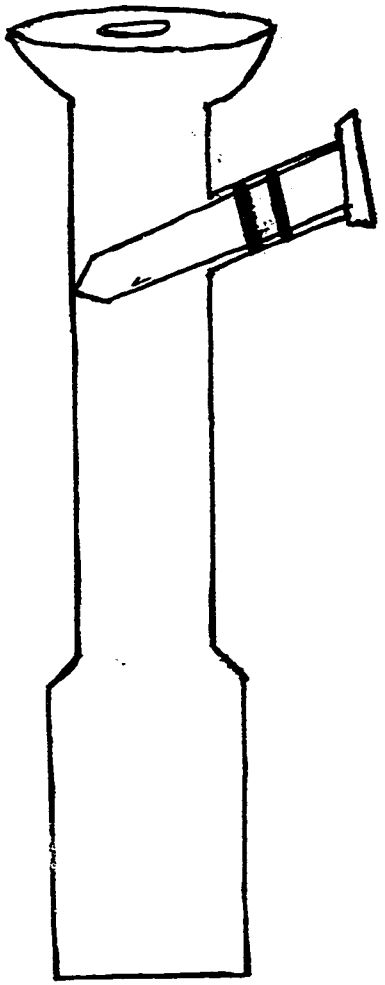

Fig. 4.--Optically flat quartz reaction cell.

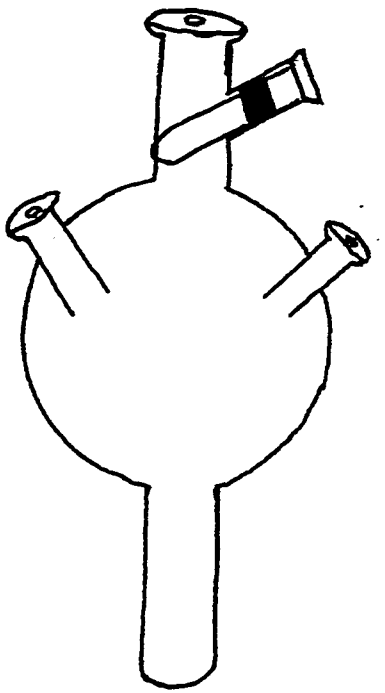

Fig. 5.--Cold finger degassing apparatus.

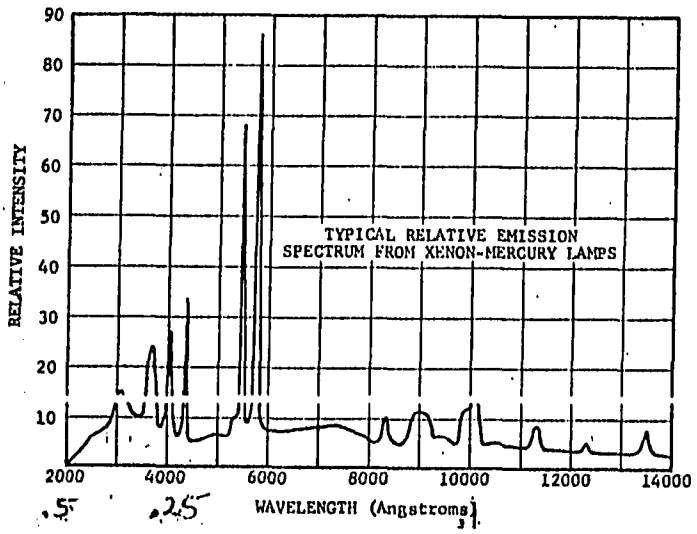

Fig. 6.--Relative Emission of Xe-Hg Lamp

TABLE 5

SPECIFICATIONS FOR Xe-Hg LAMP

Gas	Watts	Hor. Intensity (cd)	Flux (Lumens)	Average Brightness (cd/mm^2)
Xe/Hg	1,000	5,000	4,500	320

collimate the light. The collimated light beam was passed through a Corning 7-59 filter which had maximum transmittance at 366 nm, and then reflected by a mirror, positioned directly above the reaction vessel and at a 45° angle, down to the reaction vessel. In the center of the reaction vessel was a mirror mounted on a center post and set at a 45° angle with respect to the reflected light beam. The post rotated at a speed of one revolution per minute, giving equal irradiation to all cells within the vessel (Figure 7). Equal intensity at the cell positions was verified by placement of eight photoresistors (Clairex CL-703A) in the middle of eight cell compartments. The intensity of light hitting the compartments could then be compared using an oscilloscope. Figure 8 is a schematic diagram for the photoresistor setup. Figure 9 is a picture of the output from these resistors. The one peak that is larger than the others resulted from one of the photoresistors having a higher sensitivity than the others, a fact verified by exchanging the positions of the different photoresistors.

The reaction vessel was a modified circular merry-go-round in which the stationary cells were kept in a thermostated ethanol bath equidistant from the rotating mirror and the light beam. The outer wall of the vessel was blackened to prevent back reflections through the cells.

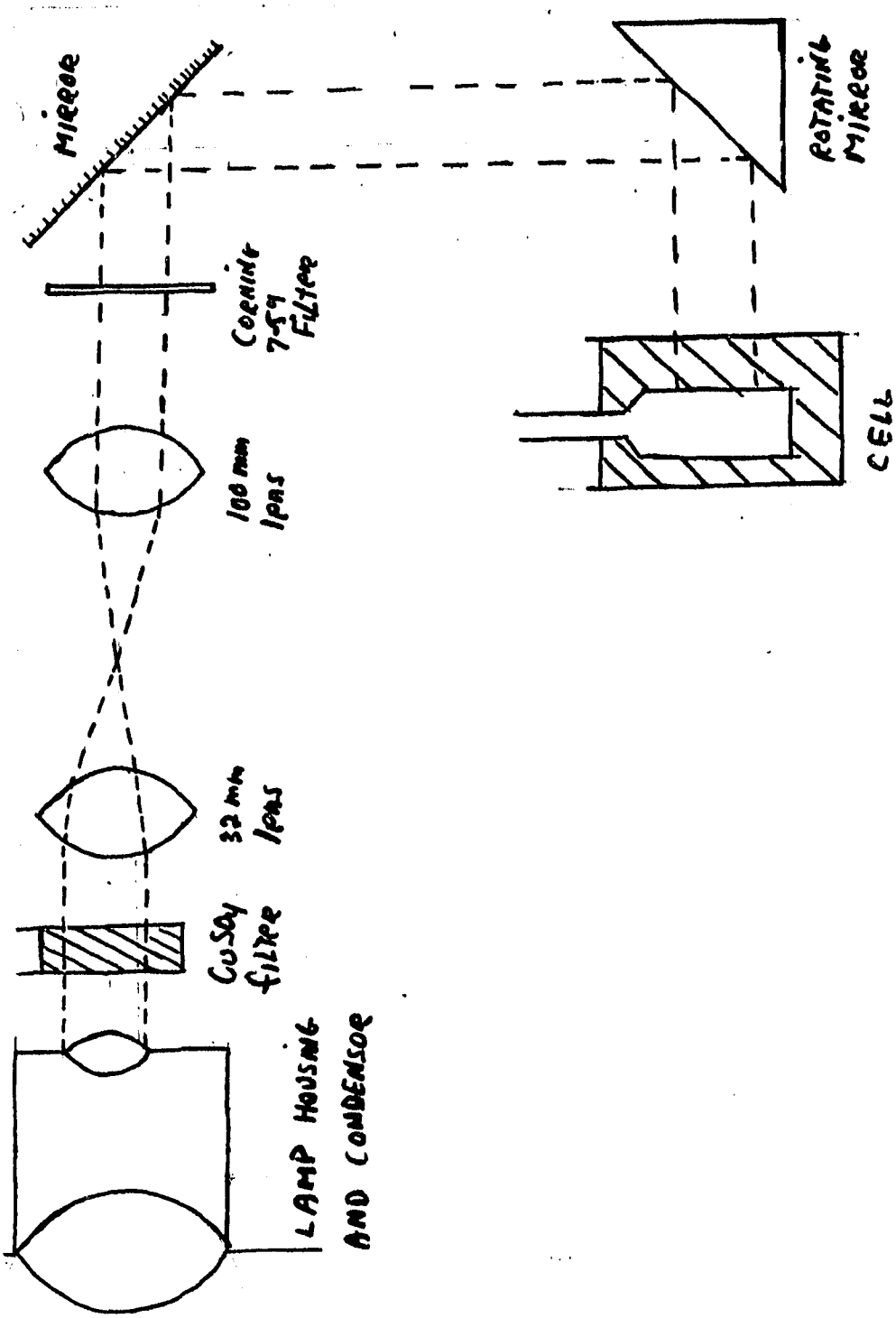

Fig. 7.--Optical Alignment Used for Irradiation

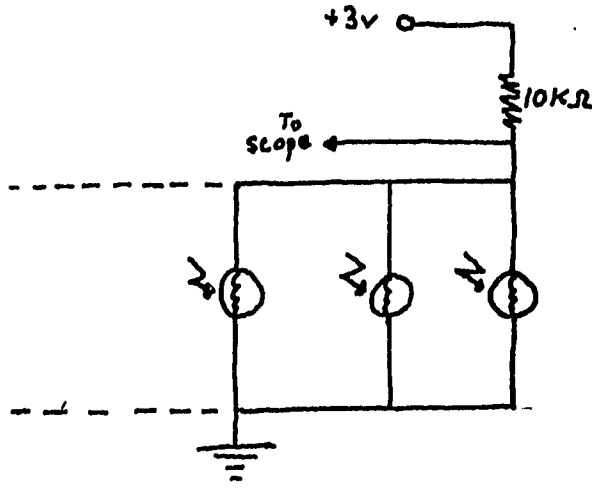

Fig. 8.--Schematic diagram for photoresistor intensity check apparatus.

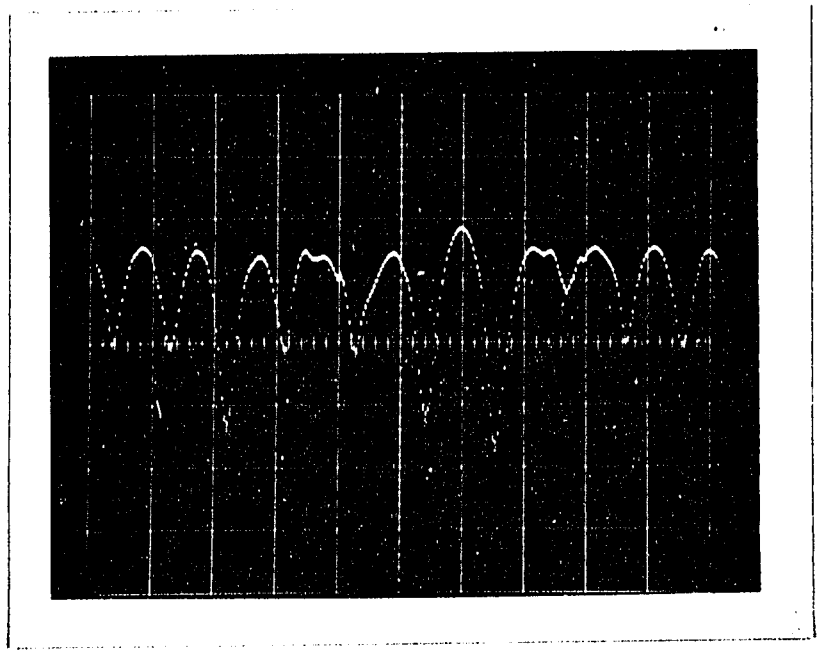

Fig. 9.--Output from photoresistors.

The aluminum cell holder was capable of holding 16 cells and could be adjusted to insure total immersion and irradiation (Figure 10).

Temperature Control

The ethanol was kept at a constant temperature in the reaction vessel by circulation through a Lauda K2 constant temperature bath. The temperature in the vessel was monitored using a 200 platinum resistance thermometer attached to a 3.5 volt regulated power supply with a resistance bridge. Readout was on a recorder (Figure 11). The linear response and calibration of the thermometer was determined using the boiling and melting points of various liquids (Figure 12). To increase the efficiency of temperature control, a vacuum jacket and several layers of glass wool were placed around the outer wall of the vessel. For temperatures below room temperature the ethanol in the constant temperature bath was circulated through a Dewar containing ice-water, dry ice-ethanol, or ethanol cooled by a Neslab Cryro-Cool immersion cooler. In cold solutions, a stream of nitrogen could be blown across the inside wall to prevent fogging. Figure 13 is a picture of the entire setup.

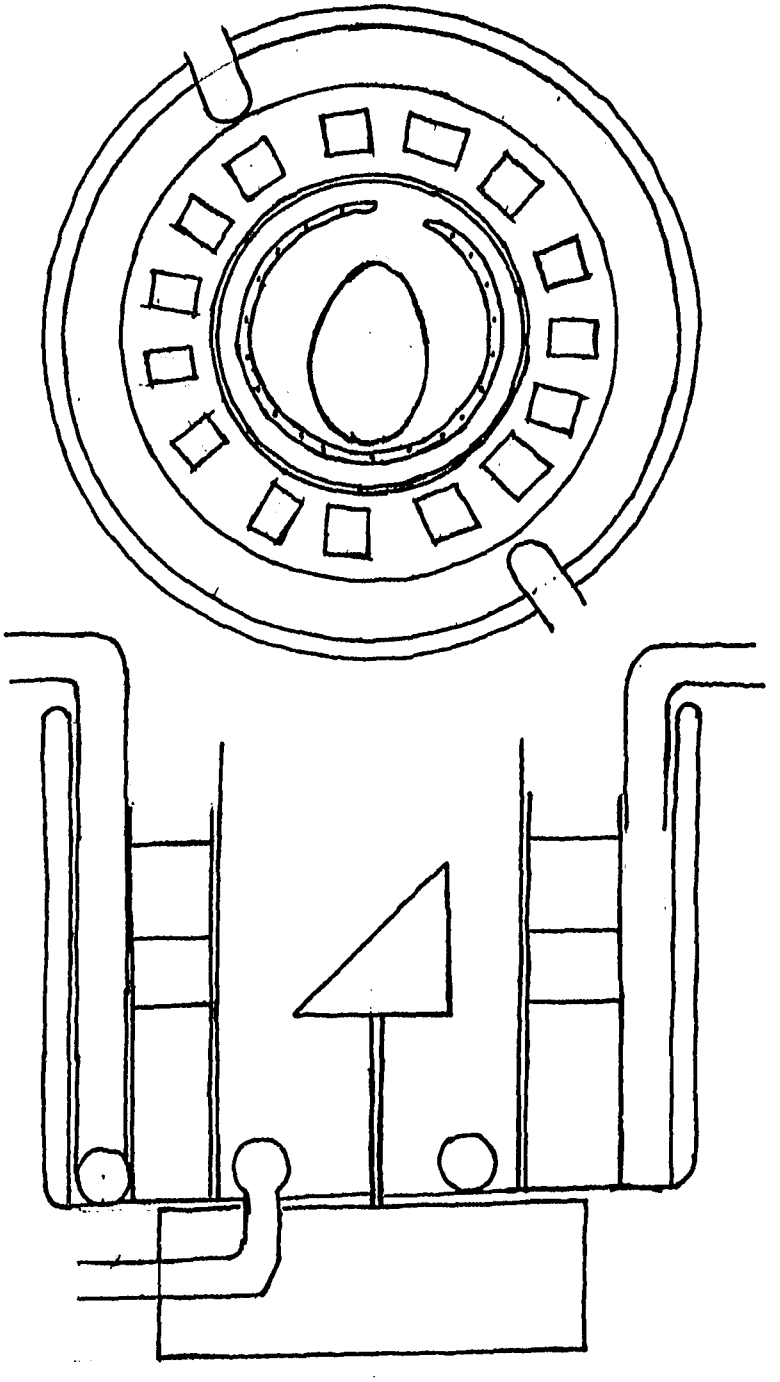

Fig. 10.--Thermostated reaction vessel.

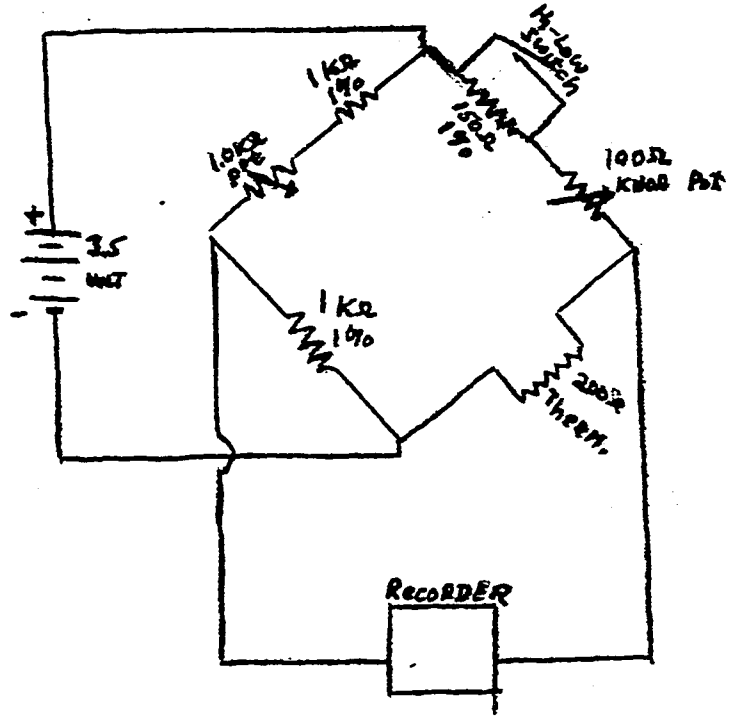

Fig. 11.--Schematic diagram for platinum resistance thermometer.

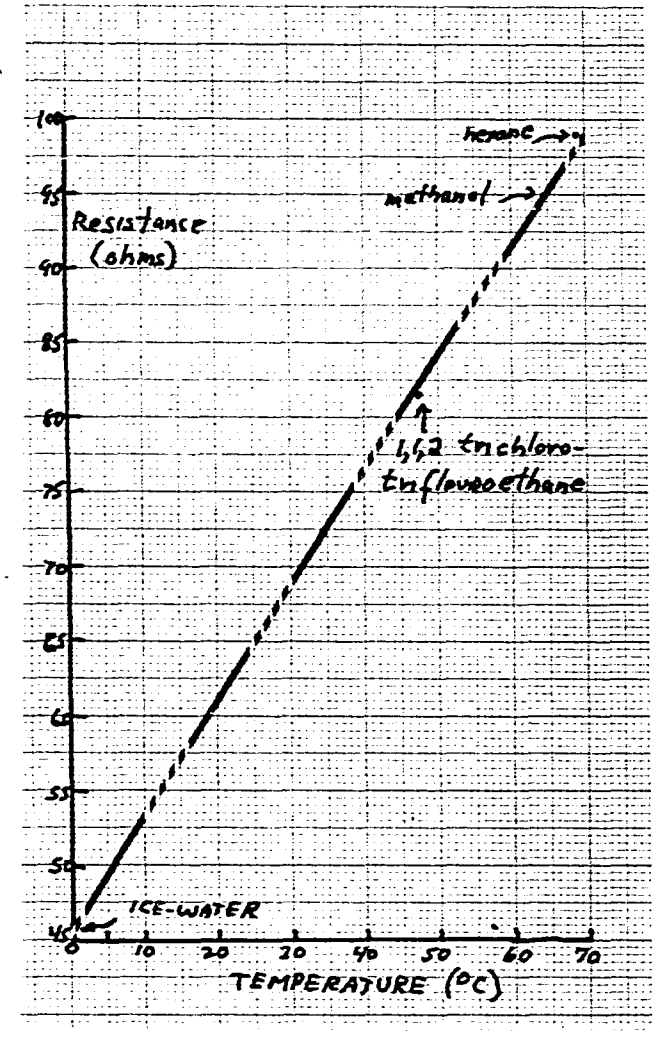

Fig. 12.--Calibration graph for resistance thermometer.

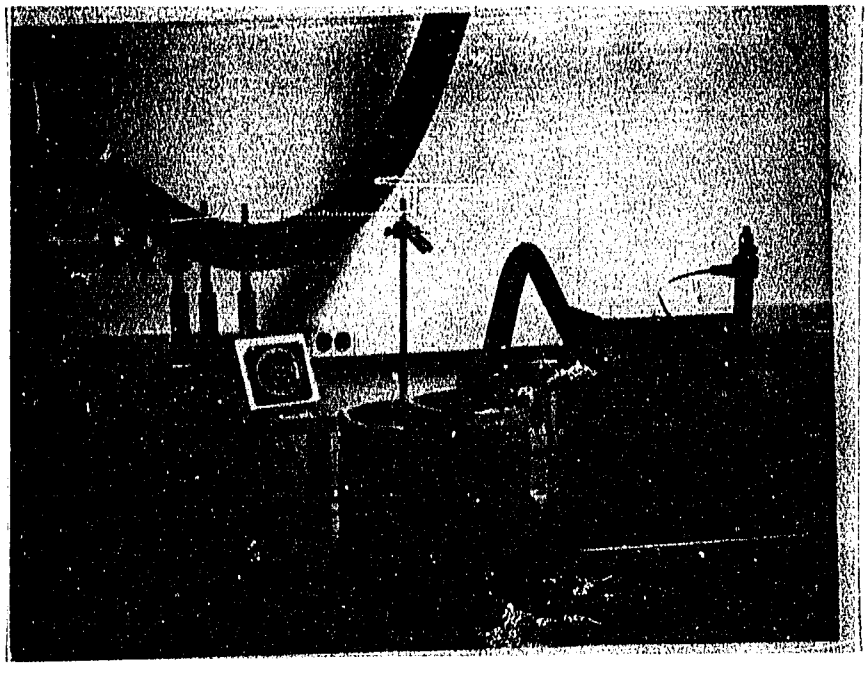

Fig. 13.--Radiation and temperature control apparatus.

Method of Determination

Absorption measurements were taken before irradiation. The cells were then placed in the reaction vessel and allowed to equilibrate to bath temperature for 15 minutes. Irradiation was initiated by removal of a shutter placed in front of the lamp and simultaneous switching on of a clock. After a period of time, the shutter was again placed in front of the lamp and the clock stopped. The cells were removed from the bath and allowed to equilibrate to room temperature for 15 minutes. Absorption measurements were again taken and the process repeated until the absorption change was 10 to 20%.

Absorption measurements were made using a Hitachi-Coleman 120 Spectrophotmeter with a Thomas digital readout attachment at 260 nm. Since the size of the cell precluded the possibility of closing the cover of the spectrometer, measurements were made by opening the shutter of the instrument in a light-tight dark room. All measurements were by difference, against an unirradiated solution of benzophenone.

Solvents and Concentrations

This section deals with those preliminary problems and experiments that were necessary to determine the best experimental design. Factors to be considered were the

concentrations of substituents and the method of preparation of the sample.

Concentrations

Solvent.--Benzene was chosen as a solvent for two reasons. The first is that almost all abstraction reactions in the literature had been run in this solvent. The second is that the yield of abstraction from the solvent is extremely low, $\phi=.02$[60]. A drawback in using benzene was its limited temperature range. However when carbon tetrachloride was used as a solvent absorption measurements were not precise enough, and 1,1,2-trichlorotrifluoroethane could not be used because of the limited solubility of benzhydrol.

Benzophenone.--The concentration of benzophenone chosen had to be large enough to insure a measurable reaction and small enough to allow absorption measurements to be taken using the reaction cell itself without having to remove the sample for dilution. The workable concentration was found to be 5.0×10^{-3}M.

Naphthalene.--The concentration of naphthalene had to be large enough to ensure that it was the dominant quenching species because of the possibility of quenching by other transient substances in the solution, yet small enough so that the rate of reaction was measurable. In a degassed solution this concentration was found to be 5.0×10^{-3}M.

Preparation of Solutions

A stock solution of 5.0×10^{-3}M benzophenone and 5.0×10^{-3}M naphthalene was used in the preparation of all benzhydrol solutions. Thus the only variable in all solutions was the concentration of the alcohol.

The original solutions tested were deaerated by bubbling for thirty minutes with oxygen-free argon. A special bubbler was constructed which allowed the solution to be deaerated and then flow into a reaction cell which had been evacuated and flushed with argon (Figure 14). However, cells prepared in this manner showed increased absorbance at 360 nm due to an intermediate described by Pitts whose absorption was in the region[94]. The system was then modified to allow the deaerated solution to flow into the degasser and go through three freeze-thaw cycles. By use of this method, a linear decrease in absorption of benzophenone with time was found but the data were not consistent or reproducible. It was then determined that consistent and reproducible results could be obtained if the solution were degassed seven times without previous deaeration.

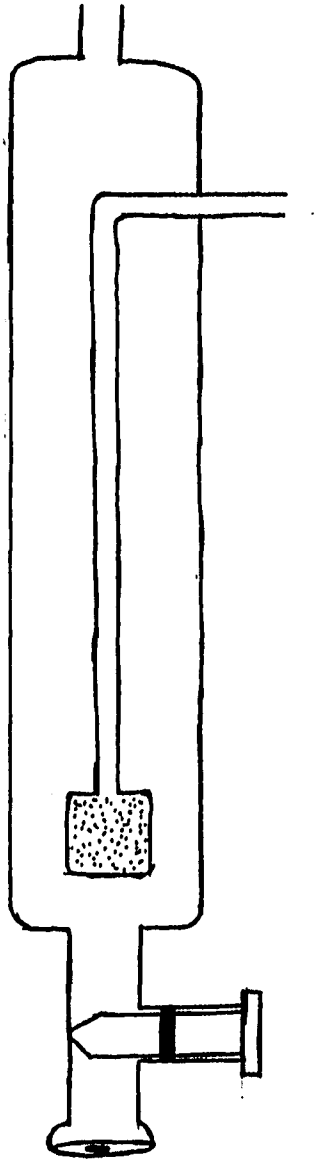

Fig. 14.--Bubbler for Aeration

CHAPTER III

RESULTS

Initial Experimental Design

Since the isotope effect is a measure of relative rates of reaction, the method of simultaneous irradiation of deuterated and non-deuterated samples provided a means of determination without the necessity of actinometry. The problem, however, was to determine the best statistical means of calculating the isotope effect and from this the best experimental design. Calculations were performed on an APL terminal of an IBM 360-50 computer.

The initial experimental design was based on the realization that if the quantum yield for the rate of benzophenone disappearance is equal in separate solutions of benzhydrol and benzhydrol-d_1 then

$$\frac{k_H[\phi_2CHOH]}{k_q[Naph]+k_d+k_H[\phi_2CHOH]} = \frac{k_D[\phi_2CDOH]}{k_q[Naph]+k_d+k_D[\phi_2CDOH]}.$$

If the solutions contain equal concentrations of quencher then

$$\frac{k_H}{k_D} = \frac{[\phi_2CDOH]}{[\phi_2CHOH]}.$$

Solutions containing equal concentrations of naphthalene and benzophenone and varying concentrations of benzhydrol or benzhydrol-d_1 were simultaneously irradiated. Absorption measurements as a function of time were taken as previously described. These measurements were normalized by dividing each result by the initial value. The least square line for each cell was then calculated.

For each line, change in absorbance values, ΔA, were calculated for 100 minutes. A least-square plot was then made of $1/\Delta A$ versus $1/[\phi_2 CHOH]$ for the solutions containing benzhydrol. From this line, the benzhydrol concentration corresponding to the $1/\Delta A$ value for the deuterated sample was then determined. The ratio of the concentration of the deuterated sample to the calculated concentration of undeuterated sample was the isotope effect.

Original runs were made with four samples of benzhydrol and one sample of d_1-benzhydrol. The temperature of the runs was 22°. The concentration range of the benzhydrol was .060 M to .12M. The concentration of the d_1-benzhydrol was 0.18M and was chosen so that its $1/\Delta A$ value would lie near the midpoint of the straight line.

Expanded Design

The number of samples used proved to be statistically too small. Therefore, the number of benzhydrol smaples was

increased to ten and the number of benzhydrol-d_1 samples was increased to four. The initial concentrations of benzhydrol were 0.0533, 0.0995, 0.151, 0.199, and 0.249M, while those for benzhydrol-d_1 were .251 and .361M. Two reaction cells were used for each concentration. To account for the increased reading error in samples of benzhydrol of low concentration, a statistical weight was given each absorbance-time curve. This was determined by the ratio of the deviation of the slope of the curve to the slope itself. Using these weights, the slope of the $1/\Delta A$ versus $1/[\phi_2CHOH]$ line was then calculated using the following formulas.

$$\text{slope} = m = \frac{\Sigma w(x-\bar{x})(y-\bar{y})}{\Sigma w(x-\bar{x})^2} \tag{18}$$

$$\text{intercept} = b = 1/\Sigma w(\Sigma wy - m\Sigma wx) \tag{19}$$

$$\sigma_y^2 = \sigma^2 = 1/N-2\Sigma w(y-m-bx)^2 \tag{20}$$

$$\sigma_m^2 = \sigma^2/\Sigma w(x-\bar{x})^2 \tag{21}$$

$$\sigma_b^2 = \sigma^2\Sigma wx^2/\Sigma w(\Sigma wx^2)-(\Sigma wx)^2 \tag{22}$$

An isotope effect value was calculated as previously described for each of the four benzhydrol-d_1 samples and an average value was taken to be the isotope effect value for that particular temperature. Table 6 is the summary of

TABLE 6

ISOTOPE EFFECT VALUES DETERMINED
BY AVERAGING METHOD

Temperature °C	Isotope Effect
8.5	2.5±0.6
16.0	2.5±0.5
16.0	2.4±0.2
22.0	2.0±0.1
46.5	2.1±0.1
58.0	2.0±0.1

results using this method for the temperature range from 8.5° to 58°. Table 7 is the APL program used.

As can be seen from Table 6, the extent of error in calculation was highly dependent on the slope of the line and on the accuracy of the $1/\Delta A$ values for the deuterated samples. A more accurate design was needed in which these errors would not be significant. It was decided that accuracy could be achieved by comparison of two lines rather than matching a point to a line.

Equation 5 shows the relationship between the quantum yield of disappearance of benzophenone and the concentration of benzhydrol. However, since

$$(23) \qquad 1/\phi = 1 + \frac{k_d + k_q[Q]}{k_{H(D)}[\phi_2 CHOH]}$$

no actinomety is being employed, the quantum yield, ϕ, is not actually being measured. What is measured is ΔA. The relationship between these two values in shown in equation 24, where a is the yield of chemically active excited state and I is the intensity of light:

$$(24) \qquad \phi = aI\Delta A$$

Equation 24 can now be rewritten as follows:

$$(25) \qquad 1/\Delta A = aI + aI \frac{k_d + k_q[Q]}{k_{H(D)}[\phi_2 CHOH]}$$

TABLE 7

APL PROGRAM FOR AVERAGING METHOD

```
      ∇LEASTSQ[⎕]∇
    ∇ LEASTSQ
[1]   'HOW MANY CELLS'
[2]   M←⎕
[3]   CELL←(M)ρ0
[4]   'THE NUMBER OF CELLS CONTAINING D-PENZHYDROL IS'
[5]   J←⎕
[6]   T←100
[7]   'ENTER X VALUES'
[8]   X←⎕
[9]   Y←((M),(ρX))ρ0
[10]  N←0
[11]  A←(M)ρ0
[12]  B←(M)ρ0
[13]  VQ←(M)ρ0
[14]  E←(M)ρ0
[15]  W←(M)ρ0
[16]  CON←(M)ρ0
[17]  OUT2←X
[18] BACK:N←N+1
[19]  'CELL NO:'
[20]  CELL[(N)]←⎕
[21]  'CONCENTRATION OF BH2'
[22]  CON[(N)]←⎕
[23]  'Y VALUES FOR CELL NO: ';CELL[(N)]
[24]  Y[(N);]←⎕ ← y[(N);] ← y[(N),] ÷ y[(N);1]
[25]  A[(N)]←X INTER Y[(N);]
[26]  B[(N)]←X SLP Y[(N);]
[27]  VQ[(N)]←X DEVSLP Y[(N);]
[28]  E[(N)]←X DEVINT Y[(N);]
[29]  W[(N)]←B[(N)]+VQ[(N)]
[30]  OUT2←OUT2,Y[(N);]
[31]  →((N)<(M))/BACK
[32]  W←W÷W[(1)]
[33]  OUT1←(M+1)ρ,0,CELL
[34]  ''
[35]  ''
[36]  LENGTH1← 3 0 6 0 6 0 6 0 6 0 6 0 6 0 6 0 6 0 6 0 6 0 6 0 6 0 6 0 6 0 6 0 6 0 6 0
```

TABLE 7--Continued

```
LENGTH1← 5 0 6 0 6 [illegible]
'CORRECTED VALUES OF ABSORBANCE'
'TIME:                    CELL NO.'
((2×(1↑))↑LENGTH1) DFT OUT1
OUT2←⍉((M+1),(ρX))ρOUT2
LENGTH2← 5 1 6 3 6 3 6 3 6 3 6 3 6 3 6 3 6 3 6 3 6 3 6 3 6 3 6 3 6 3 6 3 6 3 6 3
((2×(M+1))↑LENGTH2) DFT OUT2
OUT←⍉((6,(M))ρ,CELL,CON,B,VQ,A,E)
''
''
'CELL NO:   CONCENTRATION     SLOPE     DEVIATION   INTERCEPT   DEVIATION OF   WEIGHT'
',              OF BN2                   OF SLOPE                  INTERCEPT'
5 0 16 6 15 6 11 6 12 5 12 5 DFT OUT
''
''
→((0)=(J))/0
I←N-J
Z←(I)ρ0
G←(I)ρ0
K←(J)ρ0
L←(J)ρ0
N←0
ONCE:N←N+1
Z[(N)]←⍟(-(B[(N)]×T))
G[(N)]←⍟CON[(N)]
→((N)<(I))/ONCE
R←0
AGAIN:N←N+1
R←R+1
K[(R)]←⍟(-(B[(N)]×T))
L[(R)]←⍟CON[(N)]
→((N)<(M))/AGAIN
W←I+W
DELTA←((+/W)×(+/W×(G*2)))-((+/W×G)*2)
S←(((+/W)×(+/(W×G×Z)))-((+/W×G)×(+/W×Z)))÷DELTA
P←(÷(+/W))×((+/W×Z)-(S×(+/W×G)))
SIGSQ←(÷((ρG)-2))×(+/(W×(((Z-P)-M)*2)))
VSL←(((+/W)×SIGSQ)÷DELTA)*0.5
VP←(((+/W×(G*2))×SIGSQ)÷DELTA)*0.5
R←0
```

TABLE 7--Continued

```
[76]  Q←(J)ρ0
[77]  ISOTOPE←(J)ρ0
[78] MORE:R←R+1
[79]  Q[(R)]←(X[(R)]-P)÷S
[80]  ISOTOPE[(R)]←Q[(R)]÷L[(R)]
[81]  →((R)<(J))/MORE
[82]  ''
[83]  ''
[84]  '    1/PHI      1/PH2'
[85]  OUT3←⍉(2,(J))ρ,Z,G
[86]  10 4 10 3 DPT OUT3
[87]  ''
[88]  ''
[89]  '             CALCULATED LINE'
[90]  ''
[91]  'SLOPE  DEVIATION  INTERCEPT  DEVIATION OF'
[92]  '        OF SLOPE               INTERCEPT'
[93]  6 4 10 5 11 4 12 5 DPT,S,VSL,P,VP
[94]  ''
[95]  ''
[96]  '              ISOTOPE EFFECT'
[97]  ''
[98]  'CONCENTRATION     CONCENTRATION   ISOTOPE'
[99]  '   OF BHD            OF BH2       EFFECT'
[100] OUT4←⍉((3,(J))ρ,(÷L),(÷Q),ISOTOPE)
[101] 11 3 16 3 13 2 DPT OUT4
[102] ''
[103] ''
[104] 50 PLOT Z VS G
      ∇
```

As long as the concentration of benzophenone and naphthalene are the same in all solutions and all are irradiated with the same light, the ratio of the slopes of deuterated to undeuterated solutions is equal to the isotope effect. However, the actual value of the common intercept of both lines will depend on the intesity of the light used. Using these facts, the least-squares slopes for both the benzhydrol and benzhyrdol-d, lines were calculated for a common intercept value of -0.5 by using the formulas

$$(26) \qquad m = \Sigma wxy - b\Sigma wx / \Sigma wx^2$$

$$(27) \qquad \sigma m = (\sigma^2 / \Sigma wx^2)^{1/2}$$

The isotope effect was then calculated from the ratio of the slopes. The standard deviation for the isotope effect was then calculated from

$$(28) \qquad \sigma_{IE} = (\sigma_D^2 / m_H^2 + \sigma_H^2 m_D^2 / m_H^4)^{1/2}$$

The intercept value was then increased by 0.05 to -0.45, the slopes, isotope effect, and error were again calculated. This iteration process was continued until the isotope value with the lowest error was determined. The APL program for this method is shown in Table 8.

The isotope effect values for the previous runs was recalculated in Table 9. These values suffered from an insufficient number of data points and insufficient spread

TABLE 8

APL PROGRAM USING ITERATIVE METHOD

```
    ∇ LEASTSQ
[1]   'THE NUMBER OF THE RUN IS'
[2]   RUN←⍞
[3]   'THE TEMPERATURE OF THE RUN IS'
[4]   TEMP←⍞
[5]   'HOW MANY CELLS'
[6]   M←⍞
[7]   CELL←(M)⍴0
[8]   'THE NUMBER OF CELLS CONTAINING D-BENZHYDROL IS'
[9]   J←⍞
[10]  T←100
[11]  'ENTER X VALUES'
[12]  X←⍞
[13]  Y←((M),(⍴X))⍴0
[14]  N←0
[15]  A←B←VO←E←W←CON←(M)⍴0
[16]  OUT2←X
[17] BACK:N←N+1
[18]  'CELL NO:'
[19]  CELL[(N)]←⍞
[20]  'CONCENTRATION OF BH2'
[21]  CON[(N)]←⍞
[22]  'Y VALUES FOR CELL NO: ';CELL[(N)]
[23]  Y[(N);]←⍞
[24]  Y[(N);]←Y[(N);]÷Y[(N);1]
[25]  A[(N)]←X INTER Y[(N);]
[26]  B[(N)]←X SLP Y[(N);]
[27]  VO[(N)]←X DEVSLP Y[(N);]
[28]  E[(N)]←X DEVINT Y[(N);]
[29]  W[(N)]←B[(N)]÷VO[(N)]
[30]  OUT2←OUT2,Y[(N);]
[31]  →((N)<(M))/BACK
[32]  W←W÷W[(1)]
[33]  OUT1←(M+1)⍴0,CELL
[34]  ''
[35]  'RUN NUMBER    ';RUN;'     TEMPERATURE OF RUN= ';TEMP;' DEGREES CENTIGRADE'
[36]  ''
```

TABLE 8--Continued

```
[37]  LENGTH1← 3 0 6 0 6 0 6 0 6 0 6 0 6 0 6 0 6 0 6 0 6 0 6 0 6 0 6 0 6 0
[38]  'CORRECTED VALUES OF ABSORBANCE'
[39]  'TIME:                              CELL NO.'
[40]  ((2×(M+1))↑LENGTH1) DFT OUT1
[41]  OUT2←⍉((M+1),(⍴X))⍴OUT2
[42]  LENGTH2← 5 1 6 3 6 3 6 3 6 3 6 3 6 3 6 3 6 3 6 3 6 3 6 3 6 3 6 3 6 3
[43]  ((2×(M+1))↑LENGTH2) DFT OUT2
[44]  OUT←⍉((7,(M))⍴,CELL,CON,B,VO,A,E,W)
[45]  ''
[46]  ''
[47]  'CELL NO:   CONCENTRATION     SLOPE    DEVIATION   INTERCEPT   DEVIATION OF   WEIGH
[48]  '              OF BH2                   OF SLOPE                INTERCEPT'
[49]  5 0 16 6 15 6 11 6 12 5 12 5 11 2 DFT OUT
[50]  ''
[51]  ''
[52]  →((0)=(J))/0
[53]  I←M-J
[54]  Y←↑(-B×T)
[55]  X←↑CON
[56]  X1←I↑X
[57]  Y1←I↑Y
[58]  X2←I↓X
[59]  Y2←I↓Y
[60]  OUT3←⍉(4,(I))⍴,Y1,X1,Y2,X2
[61]  '   1/PHI    1/BH2         1/PHI    1/BH2'
[62]  9 4 8 3 13 4 8 3 DFT OUT3
[63]  SLOPE←DSLOPE←ISOTOPE←ERROR←10
[64]  C←¯5
[65]  H2←0
[66]  W1←I↑W
[67]  W2←I↓W
[68] ITER:H2←H2+1
[69]  COUNTER←0
[70]  DELTA←S←SIGSO←SIGS←2⍴0
[71]  W←W1
[72]  X←X1
[73]  Y←Y1
```

TABLE 8--Continued

```
[74] MIKE:COUNTER←COUNTER+1
[75]  DELTA[(COUNTER)]←((+/W)×(+/(W×(X*2))))-((+/W×X)*2)
[76]  S[(COUNTER)]←(+/(W×X×Y)-(C×(+/(W×X))))÷(+/(W×(X*2)))
[77]  SIGSQ[(COUNTER)]←(÷((ρX)-1))×(+/(W×(((Y-C)-S[(COUNTER)]×X)*2)))
[78]  SIGS[(COUNTER)]←(SIGSQ[(COUNTER)]÷(+/(W×(X*2))))*0.5
[79]  →((N2>1)∨(COUNTER=2))/HAPPY
[80]  SLOPE←S[(COUNTER)]
[81]  DSLOPE←SIGS[(COUNTER)]
[82]  →AVA
[83] HAPPY:SLOPE←SLOPE,S[(COUNTER)]
[84]  DSLOPE←DSLOPE,SIGS[(COUNTER)]
[85] AVA:→(COUNTER=2)/MONA
[86]  W←W2
[87]  X←X2
[88]  Y←Y2
[89]  →MIKE
[90] MONA:ISO←S[(2)]÷S[(1)]
[91]  ERR←(((SIGS[(2)]*2)÷(S[(1)]*2))+(((S[(2)]×SIGS[(1)])*2)÷(S[(1)]*4)))*0.5
[92]  ISOTOPE←ISOTOPE,ISO
[93]  EPPOR←ERROR,ERR
[94]  C←C+0.05
[95]  →(N2=1)/ITER
[96]  →((ERROR[((N2)-1)]-ERROR[(N2)])≥0)/ITER
[97]  OUT4←SLOPE[((ρSLOPE)-3)],DSLOPE[((ρSLOPE)-3)],SLOPE[((ρSLOPE)-2)],DSLOPE[((ρSLOPE)-2)],C-0.1
[98]  ''
[99]  'SLOPE OF    DEVIATION OF  SLOPE OF      DEVIATION OF   INTERCEPT'
[100] 'BENZHYDROL  BENZHYDROL    D-BENZHYDROL  D-BENZHYDROL   OF BOTH'
[101] '  LINE        SLOPE         LINE          LINE         LINES'
[102] ''
[103] 8 5 12 5 14 5 14 5 12 2 DFT OUT4
[104] OUT5←ISOTOPE[((N2)-1)],EPPOP[((N2)-1)]
[105] ''
[106] 'ISOTOPE EFFECT    ERROR'
[107] 8 2 13 3 DFT OUT5
[108] ''
      ∇
```

TABLE 9

RECALCULATED ISOTOPE EFFECT VALUES
USING ITERATIVE METHOD

Temperature °C	Isotope Effect	Standard Deviation
8.5	2.50±.20*	±0.34
16.0	2.22±.21	±0.37
16.0	2.24±.09	±0.16
22.0	1.92±.05	±0.10
46.5	1.80±.10	±0.17
58.0	1.87±.07	±0.12

*Value calculated from a t distribution with 13 degrees of freedom.

in the concentration of benzhydrol-d_1.

Four solutions of benzhydrol of concentrations 0.0622, 0.121, 0.182, and 0.239M and four solutions of newly prepared benzhydrol-d_1 of concentrations 0.122, 0.219, 0.321, and 0.424M were prepared. For each solution two cells were prepared for a total of eight data points per line. Irradiation and absorption changes were as previously described. The results obtained from these solutions are summarized in Table 10. An example of the data is presented in Table 11.

Figure 15 shows an example of the linear plots of absorption versus time for various concentrations of benzhydrol. Figure 16 shows the linear plots of $1/\Delta A$ as a function of $1/[\phi_2 CHOH]$.

TABLE 10

ISOTOPE EFFECT VALUES USING
ITERATIVE METHOD

Temperature °C	Isotope Effect	Standard Deviation
7.0	2.67±.13*	±0.23
16.5	2.55±.05	±0.10
22.0	2.64±.06	±0.12
45.0	2.58±.14	±0.26
57.5	2.10±.09	±0.17
59.5	2.18±.05	±0.11

*Value calculated from a t distribution with 15 degrees of freedom.

TABLE 11

ISOTOPE EFFECT USING ITERATIVE METHOD 22.0°C

RUN NUMBER 1934-73 TEMPERATURE OF RUN= 22 DEGREES CENTIGRADE

CORRECTED VALUES OF ABSORBANCE

TIME:	CELL NO. 21	23	13	16	10	15	17	20	9	12	18	22
0 19 24 11 14												
0.0 1.000 1.000 1.000 1.000	1.000	1.000	1.000	1.000	1.000	1.000	1.000	1.000	1.000	1.000	1.000	1.000
36.0 1.002 0.992 0.998 0.996	0.989	0.992	0.990	0.993	0.999	1.008	0.990	1.001	0.996	0.995	1.007	0.998
101.0 0.999 0.986 0.993 0.993	0.975	0.976	0.984	0.983	1.003	1.009	0.979	0.993	0.989	0.987	0.988	0.986
165.0 0.997 0.983 0.974 0.975	0.959	0.968	0.948	0.959	0.993	1.000	0.973	0.989	0.977	0.974	0.972	0.970
227.0 0.992 0.979 0.971 0.967	0.946	0.953	0.925	0.940	0.988	0.997	0.967	0.981	0.965	0.964	0.963	0.965
288.0 0.985 0.976 0.958 0.958	0.934	0.938	0.911	0.919	0.987	0.993	0.964	0.976	0.962	0.957	0.949	0.948
340.0 0.980 0.972 0.951 0.953	0.920	0.924	0.891	0.908	0.986	0.987	0.962	0.971	0.948	0.944	0.933	0.937

CELL NO:	COEFFICIENT OF PP2	SLOPE	DEVIATION OF SLOPE	INTERCEPT	DEVIATION OF INTERCEPT	WEIGHT
19	0.062200	-0.000063	0.000017	1.00325	0.00353	1.00
24	0.062200	-0.000073	0.000017	0.99817	0.00336	1.21
11	0.121000	-0.000151	0.000024	1.00287	0.00349	1.71
14	0.121000	-0.000147	0.000023	1.00182	0.00460	1.79
21	0.182000	-0.000229	0.000012	0.99825	0.00235	5.46
23	0.182000	-0.000216	0.000017	1.00029	0.00345	3.51
13	0.239000	-0.000316	0.000018	0.99877	0.00374	4.74
16	0.239000	-0.000285	0.000031	1.00454	0.00631	2.52
10	0.122000	-0.000049	0.000022	1.00174	0.00456	0.60
15	0.122000	-0.000052	0.000036	1.00776	0.00727	0.40
17	0.219000	-0.000108	0.000031	0.99826	0.00623	0.97
20	0.219000	-0.000089	0.000019	1.00210	0.00211	2.38
9	0.321000	-0.000149	0.000021	1.00168	0.00432	1.94
12	0.321000	-0.000163	0.000014	1.00134	0.00294	3.11
18	0.424000	-0.000208	0.000037	1.00772	0.00752	1.55
22	0.424000	-0.000188	0.000023	1.00329	0.00463	2.29

1/FFI	1/PP2	1/PPI	1/PPT
158.8151	16.077	203.4762	8.197
137.7455	16.077	193.0615	8.197
66.0745	8.264	92.6558	4.566
67.8903	8.264	111.7536	4.566
43.6607	5.495	66.8265	3.115
46.2563	5.495	61.2954	3.115
31.6062	4.184	47.9624	2.358
35.1194	4.184	52.8266	2.358

SLOPE OF DEUTERYDROL LINE	DEVIATION OF DEUTERYDROL SLOPE	SLOPE OF D-DEUTERYDROL LINE	DEVIATION OF D-DEUTERYDROL LINE	INTERCEPT OF BOTH LINES
8.72624	0.27887	23.02766	0.75712	-0.15

ISOTOPE EFFECT	ERROR
2.64	0.121

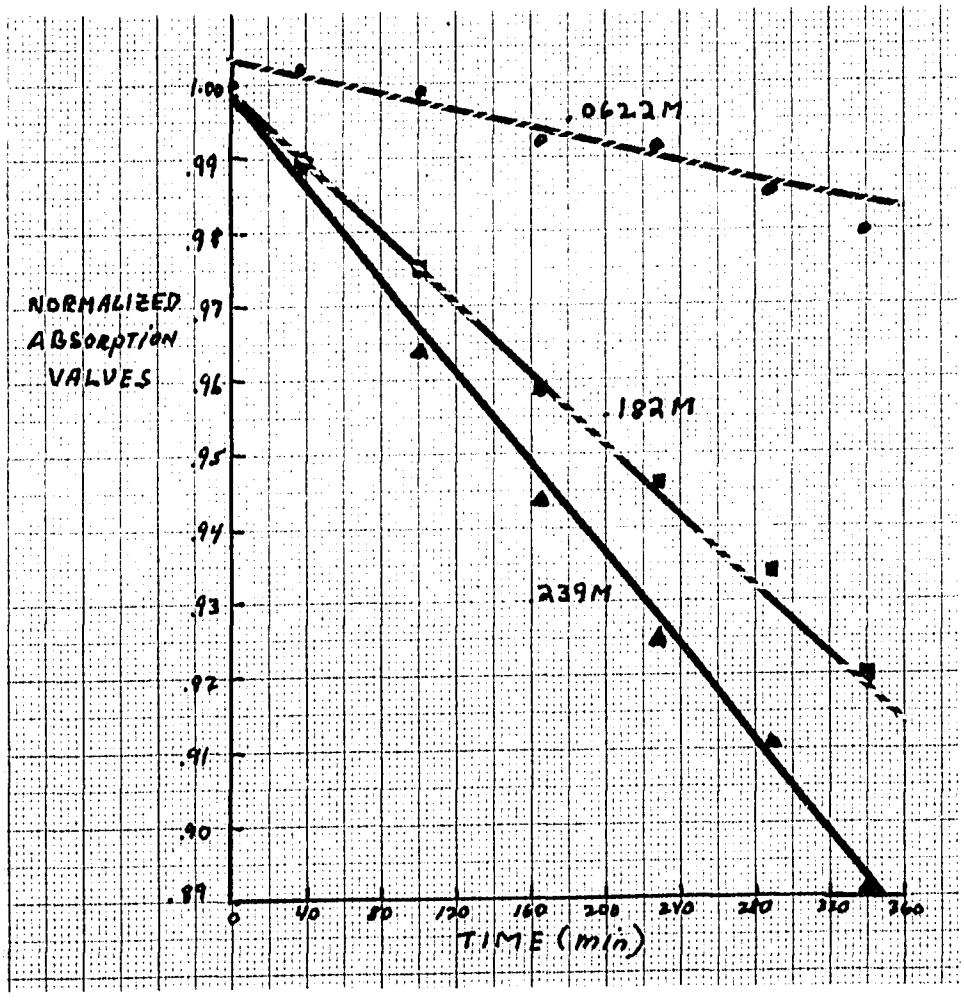

Fig. 15.--Absorption versus time curves for various concentrations of benzhydrol.

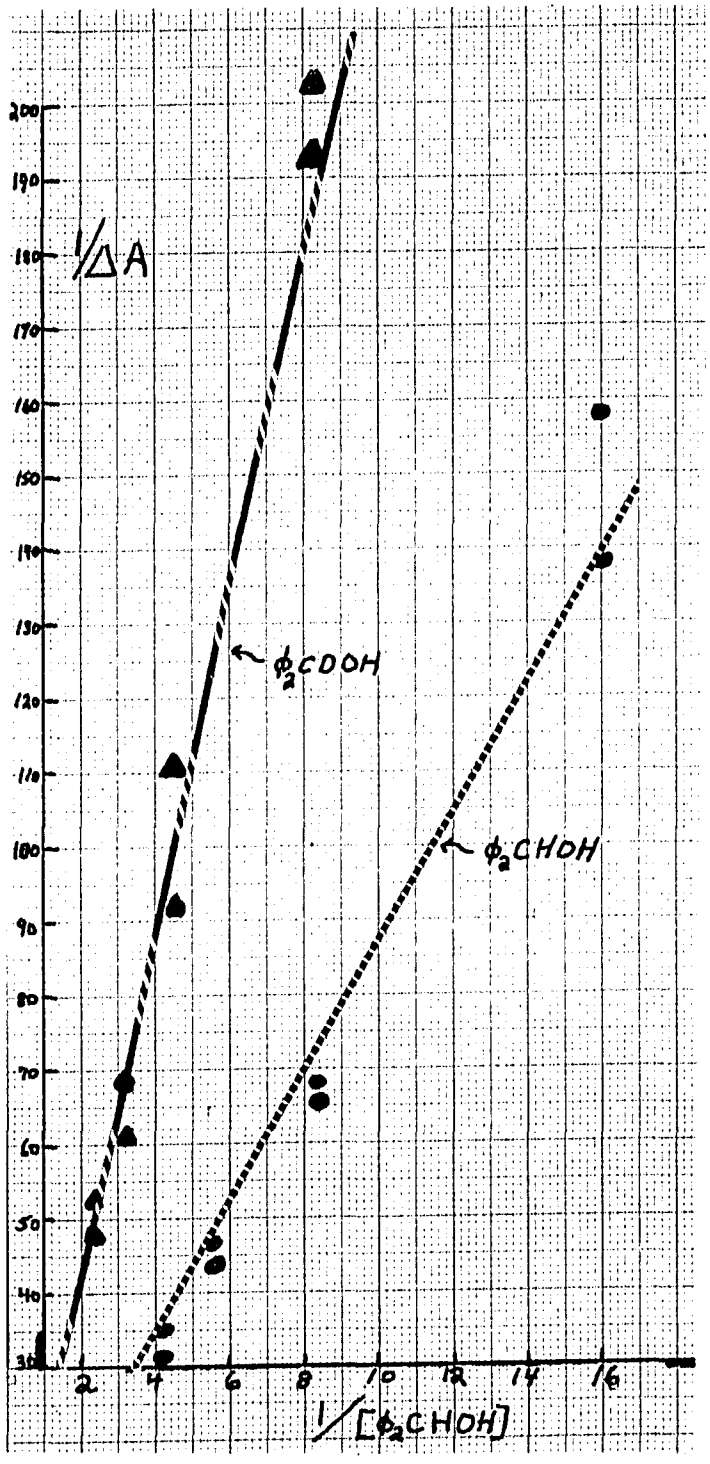

Fig. 16.--Linear plots of $1/\Delta A$ as a function of $1/[\phi_2 CHOH]$.

CHAPTER IV

DISCUSSION

Isotope effect values that were constant over the temperature range would indicate that the theories of radiationless decay were correct and the isotope effect is due to differences in vibrational overlap. A temperature dependence would indicate that the zero point energy difference or some other phenomenon was at work. Table 9 shows isotope effect values that seem to be continually decreasing as the temperature is increased. This percentage change of 33% is close to the 35% change expected from a zero point energy difference isotope effect. On the other hand, the values shown in Table 10 are constant from 7°C to 45° and then sharply decrease as the temperature is raised to 57°C. Are these trends indicative of a physical phenomenon or are they the result of random variations within the sample?

To determine whether the isotope effect values are significantly different within the temperature range studied, an analysis of variance was performed. In this test the variance of the means of each determination is compared to the variance of the total population. A ratio of this "between means" variance to the total variance would be approximately unity if the means are equal. If

the means are different, the "between means" variance will be large and the ratio will be considerably greater than unity. The extent that this ratio can be different from unity, while equality can still be assumed, is determined from a standard table. For equality of value the ratio must be smaller than the F number. To determine the ratio the following equation was used:

$$(18) \qquad \text{ratio} = \frac{\sum_{i=1}^{6} (x_i - \bar{X})^2/k-1}{\sum_{i=1}^{6} n\sigma_i^2/(N-k)} = \frac{\text{between variance}}{\text{within variance}}$$

where X_i is the isotope effect value determined at each temperature, $\bar{X}$ is the means of these values, σ_i is the error in each determination, n is the number of samples in each run, k is the number of isotope determinations made, and N is the total number of samples run.

The results of the analysis are shown in Table 12. This table shows the value of both the ratio and the corresponding F value at both the 0.05 and the 0.10 levels. In both cases it can be seen that the ratio is smaller than the F value. What this analysis indicates is that the isotope effect value cannot be shown to be different within the limits of the accuracy of the data. It does not, however, prove that the values are constant.

It is also impossible to disregard the obvious decreasing isotope effect as the temperature is increased.

TABLE 12

ANALYSIS OF VARIANCE

Run #	Mean	Variances	Ratio	F Value (.05 level)	F Value (.10 level)
#9	2.09	Between .0736 Within .0595	1.24	2.35	1.93
#10	2.46	Between .0618 Within .0331	1.87	2.33	1.92

If the assumption is made that this temperature dependence is real, the question arises as to whether it is due to an error in the theory or an uncontrolled variable in the system studied.

There is evidence that there is at least one temperature-dependent factor within the system itself that has not been considered. The assumption was made that since the quantum yield of intersystem crossing in benzophenone was unity, the only reactive or populated state was the lowest triplet. However, the existence of delayed fluorescence makes this assumption not entirely correct[65]. Because of the small energy separation between the singlet and triplet, a small percentage of the triplet electrons can be thermally excited up to the singlet state. In CCl_4 at 23°, delayed fluorescence accounted for about 10% of the total intensity of emission of benzophenone. The enthalpy was determined to be 4.4 kcal/mole, and the entropy was -3.5 eu. This led to a free energy of 5.4 kcal/mole and an equilibrium constant of $1x10^{-4}$, at this temperature. Once the singlet state is populated there can be radiative emission, radiationless decay to the ground state, or reaction with benzhydrol. The result of the first two is the addition of a temperature dependent term to k_d, the radiationless relaxation rate from the triplet state. The result of the latter is impossible to

determine, but there is no reason to believe that either the rate of reaction or the isotope effect will be the same from a reactive singlet state as that from the triplet state.

Another possible explanation for the temperature dependence might be in the omission of a secondary mechanism for energy transfer. Haas, Levine, and Stein[96] considered the possibility of energy transfer in reactions in which the extent of Franck-Condon overlap was minimized due to large energy differences between states. They postulated that during a reactive collision of the type

$$A+BC \rightarrow AB^*+C$$

there are two factors that have to be considered, a static and a dynamic displacement. The static displacement depends on curve crossing and is the usual criterion for the degree of Franck-Condon overlap, while the dynamic displacement depends on the kinetic energy of the reactive collision and on the conversion of this translational energy to electronic energy. This "extra" electronic energy can be used to decrease the separation between the two potential surfaces and increase the degree of Franck-Condon overlap. The condition for efficient energy transfer would be

$$g+d=\Delta E+m$$

where "g" and "d" are the static and dynamic displacements

respectively, "ΔE" is the electronic energy gap, and "m" is the final vibrational number.

As the temperature of the reaction system is raised the kinetic energy along the reactive pathway increases. This increased energy can lead to an increase in the efficiency of energy transfer via mechanisms not previously postulated. These include more efficient energy transfer to C-D, O-H, or C=C vibrations.

The possibility also exists that the temperature dependence of the isotope effect may be less than maximum even though caused by a zero point energy difference. As was shown in the previous section, the transition state encountered in abstraction reactions can also possess a zero point energy difference with a resulting decrease in the extent and temperature dependence of an isotope effect.

The present study was limited by the accuracy of the data. Therefore, no conclusive statement can be made about the results other than that there seems to be at least some temperature dependence. In order to determine which factors are responsible for this dependence, further experimentation is necessary. The range, especially in the low temperature region, should be expanded. Use of a second solvent, such as trifluorotoluene, may be possible.

BIBLIOGRAPHY--PART I

1. C. Hutchinson, B. Magnum, J. Chem. Phys., 32, 1261 (1960).

2. M. Wright, R. Frosch, G. Robinson, J. Chem. Phys., 33 934 (1960).

3. W. Moore, M. Ketchum, J. Amer. Chem. Soc., 84, 1368 (1962).

4. D. Coulson, N. Yang, J. Amer. Chem. Soc., 88, 4511 (1966).

5. K. Yang, J. Amer. Chem. Soc., 89, 5344 (1967).

6. (a) G. Robinson, R. Frosch, J. Chem. Soc., 37, 1962 (1962).
(b) G. Robinson, R. Frosch, J. Chem. Soc., 38, 1187 (1963).
(c) G. Robinson, J. Chem. Soc., 47, 1967 (1967).

7. (a) W. Siebrand, J. Chem. Phys., 44, 4055 (1966).
(b) W. Siebrand, J. Chem. Phys., 46, 440 (1967).
(c) W. Siebrand, D. Williams, J. Chem. Phys., 49, 1860 (1968).
(d) W. Siebrand, B. Henry, J. Chem. Phys., 49, 5369 (1968).
(e) W. Siebrand, Chem. Phys. Letters, 2, 94 (1968).

8. S. Lim, J. Chem. Phys., 44, 3759 (1966).

9. B. Henry, M. Kasha, Ann. Rev. Phys. Chem., 19, 196 (1968).

10. (a) J. Jortner, M. Bixon, J. Chem. Phys., 48, 715 (1968).
(b) J. Jortner, R. Berry, J. Chem. Phys. 48, 2757 (1968).
(c) J. Jortner, D. Chock, S. Rice, J. Chem. Phys., 49, 610 (1968).
(d) J. Jortner, D. Chock, S. Rice, J. Chem. Phys., 49, 2756 (1968).

11. B. Henry, W. Siebrand, J. Chem. Phys., 54, 1072 (1971).

12. E. Lim, Y. Li, R. Li, J. Chem. Phys., 53, 2443 (1970).

13. K. Spears, S. Rice, J. Chem. Phys., 55, 5561 (1971).

14. A. Nitzan, J. Jortner, J. Chem. Phys., 55, 1355 (1971).

15. W. Siebrand, J. Chem. Phys., 54, 363 (1971).

16. B. Selinger, W. Ware, J. Chem. Phys., 53 3160 (1970).

17. A. Brailsford, T. Chang, J. Chem. Phys., 53, 3108 (1970).

18. H. Kemper, M. Stockburger, J. Chem. Phys., 53, 268 (1970).

19. D. Heller, K. Fried, W. Gelbart, J. Chem. Phys., 56, 2309 (1972).

20. P. Johnson, L. Ziegler, J. Chem. Phys., 56., 2169 (1972).

21. W. Gelbart, K. Freed, S. Rice, J. Chem. Phys., 52, 2460 (1970).

22. (a) B. Scharf, Silbey, Chem. Phys. Letters, 5, 314 (1970).

23. S. Fischer, E. Lim, Chem. Phys., 14, 40 (1972).

24. E. Lim, H. Bhattacharjee, J. Chem. Phys., 55, 5126 (1971).

25. A. Heller, Mol. Photochem., 1, 257 (1969).

26. K. Wiberg, Chem. Revs., 55, 713 (1955).

27. L. Melander, "Isotope Effects on Reaction Rates," The Ronald Press Co., New York, N.Y., 1960, pp. 7-45.

28. F. Westheimer, Chem. Revs., 265 (1960).

29. A. Schonberg, A. Mustafa, Chem. Revs., 40, 181 (1947).

30. C. Weizmann, E. Bergmann, Y. Hirschberg, J. Amer. Chem. Soc., 60, 1530 (1938).

31. P. Wagner, G. Hammond, J. Amer. Chem. Soc., 88, 1245 (1966).

32. N. Turro, D. Weiss, J. Amer. Chem. Soc., 90, 2185 (1968).

33. S. Cohen, D. Laufer, W. Sherman, J. Amer. Chem. Soc., 86, 3060 (1964).

34. A. Beckett, A. Osborne, G. Porter, Trans. Faraday Soc., 60, 873 (1964).

35. N. Kanamuru, S. Nagakura, J. Amer. Chem. Soc., 90, 6905 (1968).

36. (a) J. Mavagkar, F. Wilkinson, Trans. Faraday Soc., 66, 2257 (1970).
(b) J. Mavagkar, F. Wilkinson, Trans. Faraday Soc., 66, 2268 (1970).

37. D. Coulson, N. Yang, J. Amer. Chem. Soc., 88, 4511 (1966).

38. N. Yang, D. Yang, J. Amer. Chem. Soc., 80, 2913 (1958).

39. N. Yang, C. Rivas, J. Amer. Chem. Soc., 83, 2213 (1961).

40. E. Zwicker, L. Grossweiner, N. Yang, J. Amer. Chem. Soc., 85, 2671 (1963).

41. E. O'Connell, Jr., J. Amer. Chem. Soc., 90, 6550 (1968).

42. N. Yang, R. Dusenberry, Mol. Photochem., 1, 159 (1969).

43. T. Godfrey, J. Hilpern, G. Porter, Chem. Phys. Letters, 1, 490 (1967).

44. S. Cohen, J. Cohen, J. Amer. Chem Soc., 89, 164 (1967).

45. G. Porter, P. Suppan, Trans Faraday Soc., 62, 3375 (1966).

46. G. Porter, P. Suppan, Trans. Faraday Soc., 61, 1664 (1965).

47. T. Godfrey, G. Porter, P. Suppan, Discussion Faraday Soc., 194 (1965).

48. A. Beckett, G. Porter, Trans. Faraday Soc., 59, 2051 (1961).

49. J. Pitts,Jr., H. Johnson Jr., T. Kuwana, J. Phys. Chem., 66, 2456 (1962).

50. V. Ermolaev, A. Terenin, Soviet Phys. Uspekhi, 3, 423 (1960).

51. G. Hammond, P. Leemakers, J. Amer. Chem. Soc., 84, 207 (1962).

52. D. Kearns, W. Case, J. Amer. Chem. Soc., 88, 5087 (1966).

53. H. Becker, J. Org. Chem., 32, 2115 (1967).

54. A Beckett, G. Porter, Trans. Fara. Soc., 59, 2038 (1963).

55. C. Walling, M. Gibian, J. Amer. Chem. Soc., 87, 3361 (1965).

56. S. Cohen, H. Chao, J. Amer. Chem. Soc., 90, 165 (1968).

57. R. Davidson, P. Lambeth, Chem. Comm., 1265 (1967).

58. (a) S. Cohen, R. Baumgarten, J. Amer. Chem. Soc., 87, 2996 (1965).
(b) S. Cohen, R. Baumgarten, J. Amer. Chem. Soc., 89, 3471 (1967).

59. S. Cohen, S. Aklipis, J. Amer. Chem. Soc., 88, 3587 (1966).

60. A. Buettner, J. Dedinas, J. Phys. Chem., 75, 187 (1971).

61. J. Dedinas, J. Phys. Chem., 75, 187 (1971).

62. G. Porter, M. Windsor, Proc. Roy. Soc. (London) Ser. A., 245, 238 (1958).

63. Y. Kanda, H. Kaseda, T. Malumura, Spectrochimica Acta, 20, 1387 (1964).

64. A. Terenin, V. Ermolaev, Trans. Fara. Soc., 52, 1040 (1956).

65. Ferguson, Tinson, J. Chem. Soc., 3083 (1952).

66. D. McClure, P. Hanst, J. Chem. Phys., 23, 1772 (1955).

67. S. Dym, R. Hochstrasser, M. Schafer, J. Chem. Phys., 48, 646 (1968).

68. D. Kearns, W. Case, J. Amer. Chem. Soc., 5087 (1966).

69. (a) J. Simpson, H. Offen, J. Phys. Chem., 52, 1467 (1970).
(b) J. Simpson, H. Offen, J. Phys. Chem., 55, 4832 (1971).

70. P. Rentzepis, Science, 169, 239 (1970).

71. R. Hochstrasser, J. Chem. Phys., 1038 (1964).

72. P. Rentzepis, M. Topp, Trans. of N.Y. Acad. of Science, Ser. II, 289 (1971).

73. A. Lamola, G. Hammond, J. Chem. Phys., 43, 2129 (1965).

74. T. Nakamura, S. Hayakawa, Japanese Journal of Applied Phys., 8, 85 (1969).

75. J. Saltiel, H. Curtis, L. Metts, J. Miley, J. Winterle, M. Wrighton, J. Amer. Chem. Soc., 92, 410 (1970).

76. W. Clark, A. Litt, C. Steel, J. Amer. Chem. Soc., 91, 5413 (1969).

77. C. Parker, T. Joyce, Chem. Comm., 749 (1968).

78. G. Hammond, W. Baker, W. Moore, J. Amer. Chem. Soc., 83, 2795 (1961).

79. P. Wagner, Mol. Photochem., 1, 71 (1969).

80. F. Minn. C. Trichilo, C. Hunt, N. Filepscu, J. Amer. Chem. Soc., 92, 3600 (1970).

81. S. Weiner, J. Amer. Chem. Soc., 93, 425 (1971).

82. C. Warnser, G. Hammond, C. Chang, C. Baylor, J. Amer. Chem. Soc., 92, 6362 (1970).

83. W. Moore, G. Hammond, R. Foss, J. Amer. Chem. Soc., 83, 2789 (1961).

84. J. Bell, H. Linschitz, J. Amer. Chem. Soc., 85, 528 (1963).

85. H. Tsubomuna, N. Yamamoto, S. Tanaka, Chem. Phys. Letters, 309 (1967).

86. G. Porter, F. Wilkinson, Trans. Fara. Sco., 57, 1686 (1961).

87. J. Farmer, C. Gardner, C. McDowell, J. Chem. Phys, 34, 1058 (1961).

88. H. Backstrom, K. Sandros, Acta Chem. Scand., 14, 48 (1960).

89. P. Wagner, J. Amer. Chem. Soc., 89, 2820 (1967).

90. G. Hammond, R. Foss, J. Phys. Chem., 68, 3739 (1964).

91. (a) S. Cohen, S. Orman, D. Laufer, J. Amer. Chem. Soc., 1061 (1962).
(b) S. Cohen, S. Orman, D. Laufer, J. Amer. Chem. Soc., 84, 3905 (1962).

92. R. Davidson, P. Lambeth, Chem. Comm., 511 (1968).

93. "A Specialist Periodical Report, Photochemistry," Vol. 3, The Chemical Society, p. 626 (1972).

94. J. Pitts, R. Letsinger, R. Taylor, J. Patterson, G. Wald, R. Martin, J. Amer. Chem. Soc., 81, 1068 (1959).

95. R. Steward, J. Amer. Chem. Soc., 82, 6168 (1960).

96. Y. Haas, R. Levine, G. Stein, Chem. Phys. Letters, 15, 7 (1972).

PART II

THE PHOTOVOLTAIC EFFECT OF $K_4Mo(CN)_8$

CHAPTER I

INTRODUCTION

Navidi, Brittain, and Heller[1] found that irradiation of a solution of molybdenum (IV) in a pyrex half-cell connected to a dark half cell produced a voltage. The cells were thermostated in a water bath and irradiated through this bath with a halogen lamp. The molybdenum compound was prepared by mixing an equivalent of $(NH_4)_6Mo_7O_{24}\cdot 4H_2O$ with two equivalents of $(NH_4)_2MoCl_5\cdot H_2O$. The possibility was presented that this voltage might be due to the production of an aquated electron with the reaction on the illuminated half-cell being

$$Mo(IV) \xrightarrow{h\nu} MO(V) + e^-$$

and the reaction on the dark side being

$$Mo(IV) + e^- \rightarrow Mo(III)$$

However, some of the questions that arose could not be answered on the basis of the initial experiment. The compound originally used was not stable so that some of the voltage could have been due to a thermal reaction. Moreover, irradiation was with light of wavelengths greater than 3000 A°, much too low in energy for photoejection of an electron. It seemed apparent that this phenomenon required

examinations under more controlled conditions with a more stable molecule.

Photochemistry of Inorganic Complexes

The lack of emission from the excited states of most inorganic molecules makes the photochemical processes occurring in inorganic complexes difficult to determine. In general, electronic states can be separated into five categories: ligand field, charge transfer to ligand (CTTL), charge transfer to metal (CTTM), and charge transfer to solvent (CTTS). Ligand field transitions are those involving excitation within the nondegenerate d orbitals of the complex. Since these nondegenerate d orbitals are directed toward the ligands, excitation will increase the electron density at these positions and consequently increase the degree of repulsion between the central atom and the ligand. The probability of the loss of a ligand by substitution or elimination becomes more likely[2]. Charge transfer to metal bands occurs in complexes with high reducing ligands such as Br^- and I^-. Charge transfer to ligand occurs with central atoms with low ionization potentials and ligands with empty π^* orbitals such as CN^- and CO^2.

In charge-transfer excitation the assumption is made that the molecular orbitals of the central atom, ligands and solvent are separate systems with only weak interaction. The central atom has a definite oxidation number

and excitation from the central atom to the ligand, or the reverse, results in a change in this oxidation number. Several types of reactions are possible from these states, including intramolecular and intermolecular oxidation-reduction and substitution reactions.[2]

A recently discovered reaction, the formation of an aquated electron, occurs in the irradiation of certain inorganic cyanide complexes such as $Fe(CN)_6^{4-}$ [3-5], $Mo(CN)_8^{4-}$ [6-8], with $Fe(CN)_6^{4-}$. Photoejected electrons have also been discovered above the surface of the solution[9,10]. The criteria for photoejection of an electron from a molecule are (1) irradiation in the charge-transfer band of the molecule, (2) a stable molecule of the same stoichiometry and one higher oxidation number than the original molecule, and (3) a stable molecule of one lower oxidation number[6-7] as the original molecule.

It was originally believed that the source of the electron was the CTTS state reached as the primary step of excitation. However, recent studies on the effect of temperature, ionic strength, and added D_2O on the quantum yield of electron formation from $Fe(CN)_6^{4-}$ indicate that the CTTS state is reached by a secondary process. Excitation to the high-energy ligand field $^1T_{2g}$ state at 2700 A° or the CTTL $^1T_{2u}$ state at 2180 A° results in internal conversion to the lower energy $^1T_{1g}$ state at 3225 A° where a substitution

reaction occurs. Competing with relaxation is crossing, possibly by tunneling, to a CTTS state with the formation of an aquated electron[4,5]. A similar mechanism is believed to occur in $Mo(CN)_8^{4-}$ and $W(CN)_8^{4-}$ since they both contain a high-energy CTTL state.[5]

Photochemistry of $K_4Mo(CN)_8$

The symmetry of $K_4Mo(CN)_8$ has been called fluxional. Under different conditions the symmetry has been determined to be either D_{2h}, square antiprism, or D_{4h}, dodecahedron[11]. Spectral data for the $K_4Mo(CN)_8$ molecule have been determined by Perumareddi, Liehr, and Adamson[12] and are shown in Table 1 and Figure 1. $K_4Mo(CN)_8$ is thermally stable but photochemically active. Depending on the energy of excitation, two distinct photochemical reactions are observed. First, irradiation of a degassed aqueous solution with light of wavelength less that 3000 A° results in the formation of an aquated electron. The electron can be detected by its reaction with N_2O producing N_2;[7]

$$Mo(CN)_8^{4-} \xrightarrow{-h\nu} Mo(CN)_8^{3-} + e^-_{aq}$$

$$e^-_{aq} + H_2O + N_2O \rightarrow N_2 + \cdot OH + OH^-$$

$$\cdot OH + Mo(CN)_8^{4-} \rightarrow Mo(CN)_8^{3-} + OH^-$$

The quantum yield of N_2 formation has been determined

TABLE 1

SPECTRAL DATA FOR THE d^2 - TRANSITION METAL CYANIDE COMPLEX ANIONS[12]

λ_{max} nm	υ_{max} cm^{-1}	ε_{max}	Assignment	Calcd. Frequency cm^{-1}
-	-	-	$^1A_1 \rightarrow {}^3A_2$	17,925
510.0	19,600	2.7	$^1A_1 \rightarrow {}^3B_1$	19,625
431.0	23,200	69	$^1A_1 \rightarrow {}^1A_2$	23,175
-	-	-	$^1A_1 \rightarrow {}^3E$	25,550
-	-	-	$^1A_1 \rightarrow {}^3E^1$	28,750
367.6	27,200	170	$^1A_1 \rightarrow {}^1B_1$	27,875
308.2	32,450	262	$^1A_1 \rightarrow {}^1E$	33,050
267.4	37,400	1,350	$^1A_1 \rightarrow {}^1E^1$	36,050
240.0	41,670	15,540	Charge Transfer	

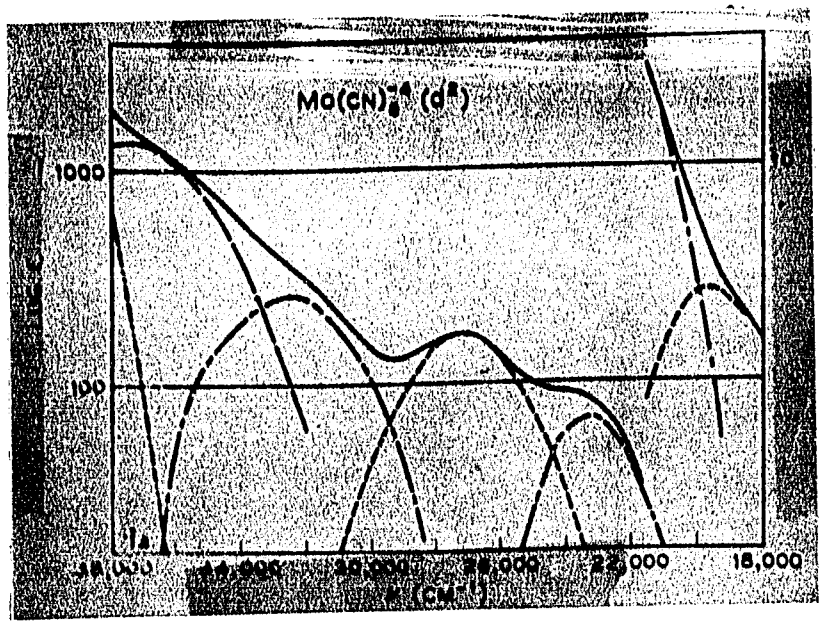

Fig. 1--Spectrum of $Mo(CN)_8^{4-}$

to be 0.27[7]. The rate of the back reaction

$$Mo(CN)_8^{3-} + e_{aq}^- \rightarrow Mo(CN)_8^{4-}$$

has been found to be 4.0×10^8 sec^{-1} [7]. In the presence of N_2O, secondary products such as $Mo(CN)_7H_2O^{2-}$ and $Mo(CN)_7H_2O^{3-}$ have been detected[7]. However, it is not certain whether the •OH radical is responsible for their formation. The electron has also been detected by its absorption at 6800 A° during flash photolysis[6]. It is still not clear whether the mechanism of electron ejection is a secondary process as in $Fe(CN)_6^{4-}$ or is direct population of the CTTS state.[8]

Second, excitation in the ligand band of the compound with light above 3000 A° causes the original yellow solution to turn to red, then green, and finally blue[14,15,16]. The pH of the solution also increases[15,16]. The initial reaction is[16]

$$Mo(CN)_8^{4-} + 2H_2O \xrightarrow[>3000A°]{h\nu} Mo(CN)_7^{3-} + HCN + OH^-$$

The red intermediate, $Mo(CN)_7H_2O^{3-}$, has been isolated as the silver salt by addition of solid $AgNO_3$ during irradiation of an acidic solution of the complex[17]. The growth and decay of this intermediate has been followed by its absorption at 5120 A° and by polarography[18]. The final product has been isolated as a red solid by addition of

solid KOH to the blue solution at 0°[19]. This solid has been identified as transdioxytetracyanomolybdate, (IV), $MoO_2(CN)_4^{4-}$. The red solid turns blue on addition of water because of the equilibrium

$$MoO_2(CN)_4^{4-} + H_2O \rightleftarrows MoO(OH)(CN)_4^{-3} + OH^-$$

Although the intermediate and the final product have been isolated, the detailed mechanism is still in doubt. The initial step is reversible as long as the red intermediate is present; however, the exact steps from red intermediate to final product are speculative. In the photolysis of $(NH_4)_4Mo(CN)_8$ in liquid ammonia, a postulated multi-photon process was necessary to produce the final polymeric product[20].

CHAPTER II

EXPERIMENTAL

Chemical

$K_4Mo(CN)_8$. Potassium octacyanomolybdate was prepared by three different methods to insure that the results obtained were not due to an impurity formed during preparation.

Method 1--This method was adopted from a method described by Palmer[21] with only slight modification. A 10% solution of MoO_3 in 75 ml of 8N HCl was reduced to Mo(III) at a mercury cathode using 1.5 to 2 amps. Reduction took 4-5 hours. The reduced solution was then discharged into a solution of half the molar quantity of MoO_3 in an N_2 atmosphere producing a dark red chloride complex of Mo(IV).

$$2Mo(III) + Mo(VI) \rightarrow 3Mo(IV).$$

The complex was treated with 48 g of NH_4CNS, 30 ml pyridine, and 7.5 M NH_3 to form a red oil whose probable formula is $py_2H_2Mo(NCS)_6$. The oil was solidified by cooling. The solid was added to a solution of 50 g of KCN dissolved in 65 ml of hot water. Pyridine was removed by bubbling with steam. The product was isolated as the sparingly soluble $Cd_2Mo(CN)_8 \cdot 2H_2O$ and crystallized by addition of ethanol.

The yield after recrystallization was 5.0 g.

Method 2--This method is similar to the above method except that $MoCl_4$, obtained from Research Organic/Inorganic Chemical Corp., was used rather than the reduced solution.

Method 3--In the third method, adopted from Schlessinger[22], 250 ml of a concentrated HCl solution was added dropwise to 50 g of MoO_3 dissolved in 150 ml of a 30% KOH solution until a cream-colored suspension of H_2MoO_4 was produced. The suspension was heated with 150 g KCNS producing the blood red $MoO_2(SNC)_2$ which was then heated with pyridine to produce $MoO_2(SNC)_2$-2py. When the pyridine complex was heated with 200 g KCN and then cooled, the crude cyanide complex was formed. The product was purified first with activated charcoal and then by repeated water-ethanol recrystallizations. The yield was 23 g.

$K_4MoO_2(CN)_4$: Potassium transoxytetracyanomolybate (IV) was prepared by irradiation of a solution of $K_4Mo(CN)_8$ using a medium-pressure mercury lamp until the solution turned dark blue. Solid KOH pellets were added and the solution was cooled until red crystals of the salt precipitated.[19] These crystals were filtered. Purification was achieved by redissolving them in water and then recrystallizing them with KOH.

Photovoltaic Effect

The photovoltaic cell. The photovoltaic cell used in these experiments was similar to the one used by Navidi[1]. The half-cells were six-inch long pyrex tubes 2-mm thick. The tubes were connected by a glass fritted disk halfway up the tube. Each half-cell contained a thin pyrex tube leading to the bottom used to bubble nitrogen through the solutions during irradiation. Conditioned platinum wires were used as electrodes in each half-cell. Conditioning was accomplished by electrolyzing each wire in a concentrated nitric acid solution prior to use. The electrodes were held in place by pushing them through the midpoint of a stopper. The stoppers were then placed at the top of each half-cell in such a manner that the electrodes were in the center of the cell and at the point where light would hit the cell. They were then externally connected through a Digillin 100 megaohm digital millivoltmeter (Figure 2).

Optical system. Irradiation was performed using an Hanovia 150-watt Xe lamp powered by a Solar power supply. The light was passed through two pyrex lenses, an ir filter, and a circular slit forming a collimated light beam the width of one half-cell. The other half-cell was covered with aluminum foil.

Method of determination. Before irradiation was

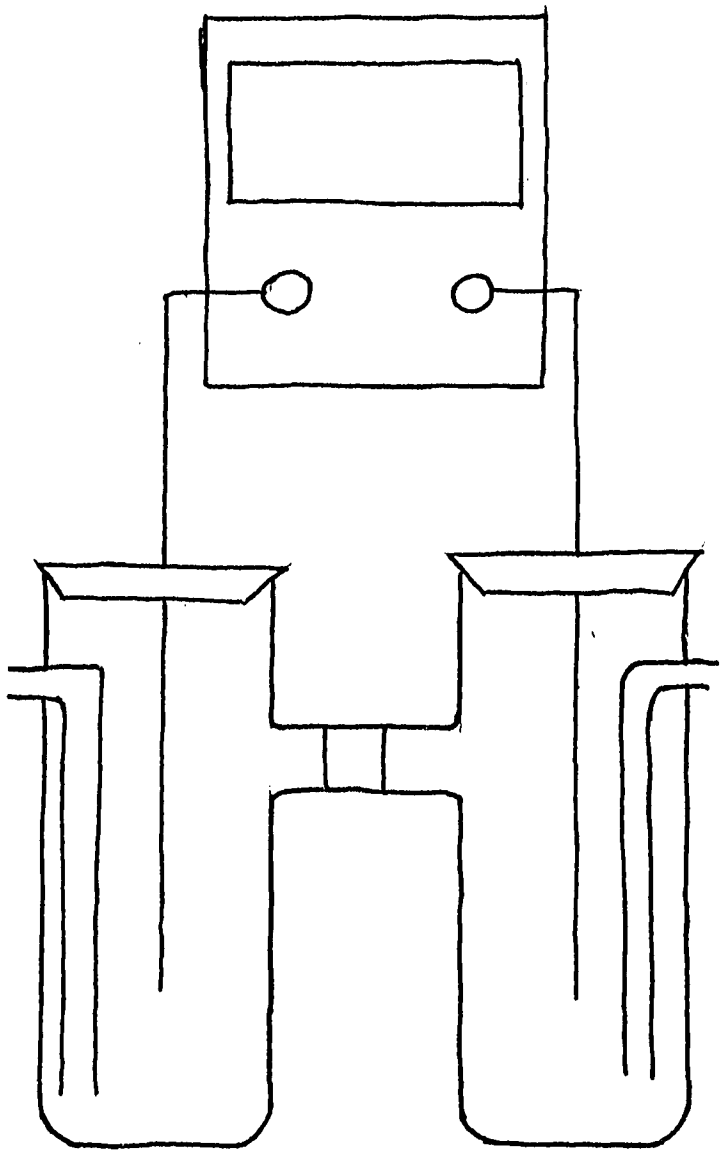

Fig. 2.--Photovoltaic Cell

initiated, nitrogen was bubbled through both solutions for at least 15 minutes to equilibrate and deaerate the solutions. Equilibration was achieved when the millivoltmeter indicated zero potential between the half-cells for at least 5 minutes. During this same period the lamp was turned on, but was shuttered to prevent the light from hitting the cell. Irradiation was initiated by simultaneous removal of the shutter and switching on of a timer capable of reading ±0.05 minutes. Voltage readings were initially taken every tenth minute until the potential change decreased enough for readings to be taken at shorter intervals.

The concentration of $K_4Mo(CN)_8 \cdot 2H_2O$ solution was 2.0×10^{-3}M and the solution was buffered at pH 9.0 by addition of 100 mg borax. Solutions were made and stored in the dark.

Polarographic Studies

Polarographic and photochemical cell. Polarograms were taken on a three-electrode Beckman Electroscan 30. The reference electrode was platinum, the standard electrode a calomel electrode, and the working electrode a dropping mercury electrode with a mercury height of 50 cm and a drop time of four seconds. Irradiation and polarograms were conducted simultaneously in a cylindrical cell with an outer water jacket which served the dual role of ir filter and constant temperature bath. The temperature was kept at

25° for all runs. A dual purpose bubbler was used initially to deaerate the solution and then to keep a blanket of nitrogen over the solution. A filled neoprene cover was used to keep a closed system and to hold the electrodes and bubbler in position (Fig. 3). The entire cell was blackened excepted for a one-inch circular window which allowed the passage of light to the solution. The mercury electrode was placed in front of this window during irradiation.

Method of determination. For each run fresh solutions were prepared in the cell. They contained 20 g $K_4Mo(CN)_8 \cdot 2H_2O$, 100 g Borax buffer, 20 ml of 2M $KClO_4$ or 20 ml 1M KCl, 5 ml Triton X-100 and 50 ml glass distilled water. Solutions were bubbled with nitrogen for 20 minutes prior to irradiation. To insure that the solution was oxygen free, a polarogram from zero to minus 1.9 volt was done. During this time bubbling was stopped but a flow of nitrogen was kept through the cell. The absence of the dual oxygen waves at -0.1 volt and -0.9 volts indicated that aeration was complete.

Measurements during irradiation were performed in one of two ways. The solutions were either bubbled or not bubbled with nitrogen. If nitrogen was not bubbled through the solution, measurements were made during the total span of irradiation. If bubbling was used, measurements could only be made at set intervals during which bubbling was

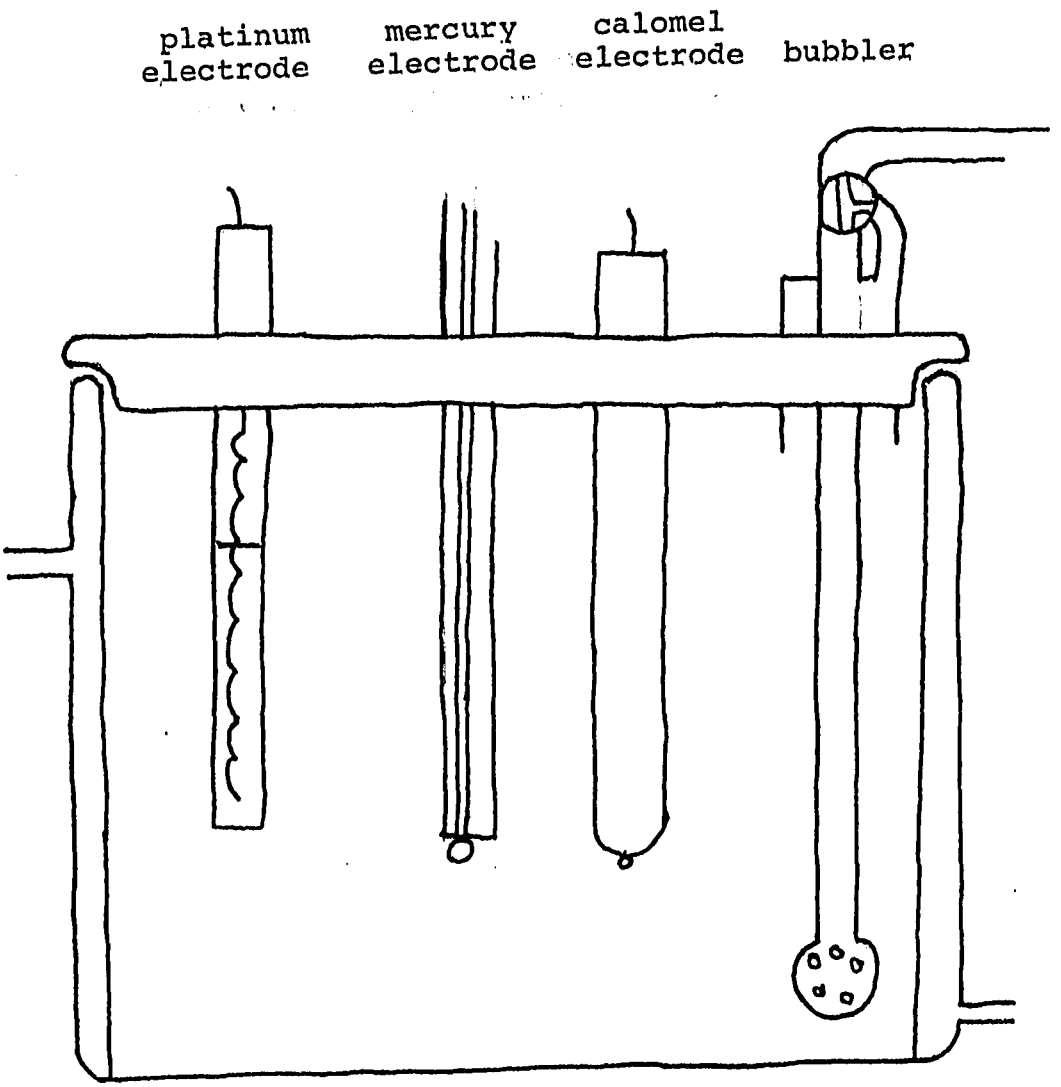

Fig. 3.--Polarographic and Photochemical Cell

terminated. Under both conditions the current was measured either by scanning over a potential range between 0 and -1.8 volts or by sitting on a set potential and following the current change with time.

CHAPTER III

RESULTS

Photovoltaic Effect

A potential was instantaneously produced when irradiation was initiated with the irradiated half-cell as the negative electrode. The potential change was rapid initially, began to decrease when the solution turned red, and became zero when the solution was green. The potential then stayed constant even after several hours of irradiation (Figure 4). During the initial period of irradiation the potential change was reversible. Termination of illumination caused the potential to approach zero. Initiation again produced a rapid potential change. At no time was there a change in the solution in the dark half-cell.

Results were qualitatively but not quantitatively reproducible. Irradiation of two solutions of exactly the same concentration produced similar qualitative results except that the rate of change of potential and final potential were different. Figure 5 shows the voltage change for two molybdate solutions of exactly the same concentration. Although the shape of both curves and that of I (Figure 4) are similar, they all differ in the initial rate of rise and in the voltage reached in the plateau.

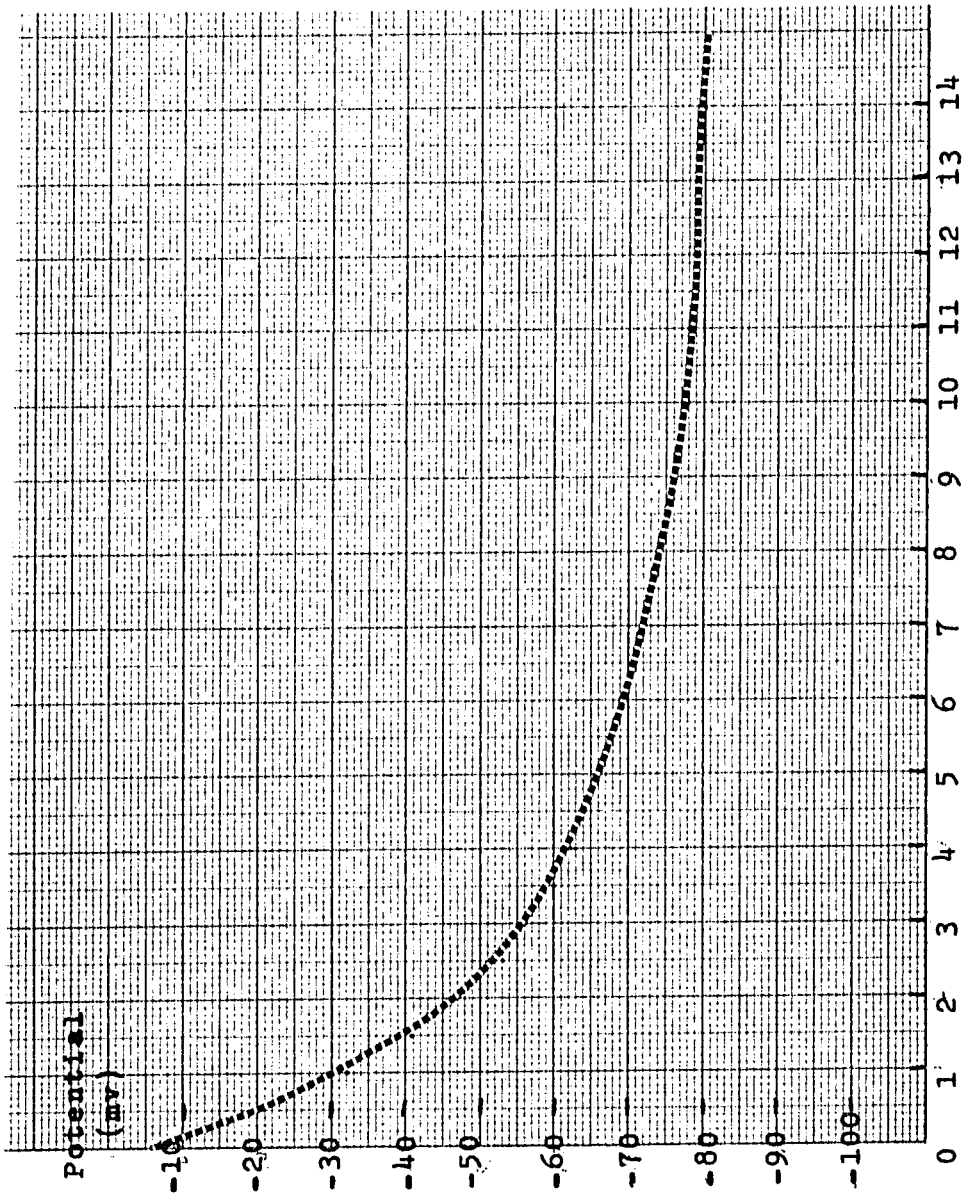

Fig. 4.--Potential Change of Irradiated $K_4Mo(CN)_8$ with Time (Conditions described in text)

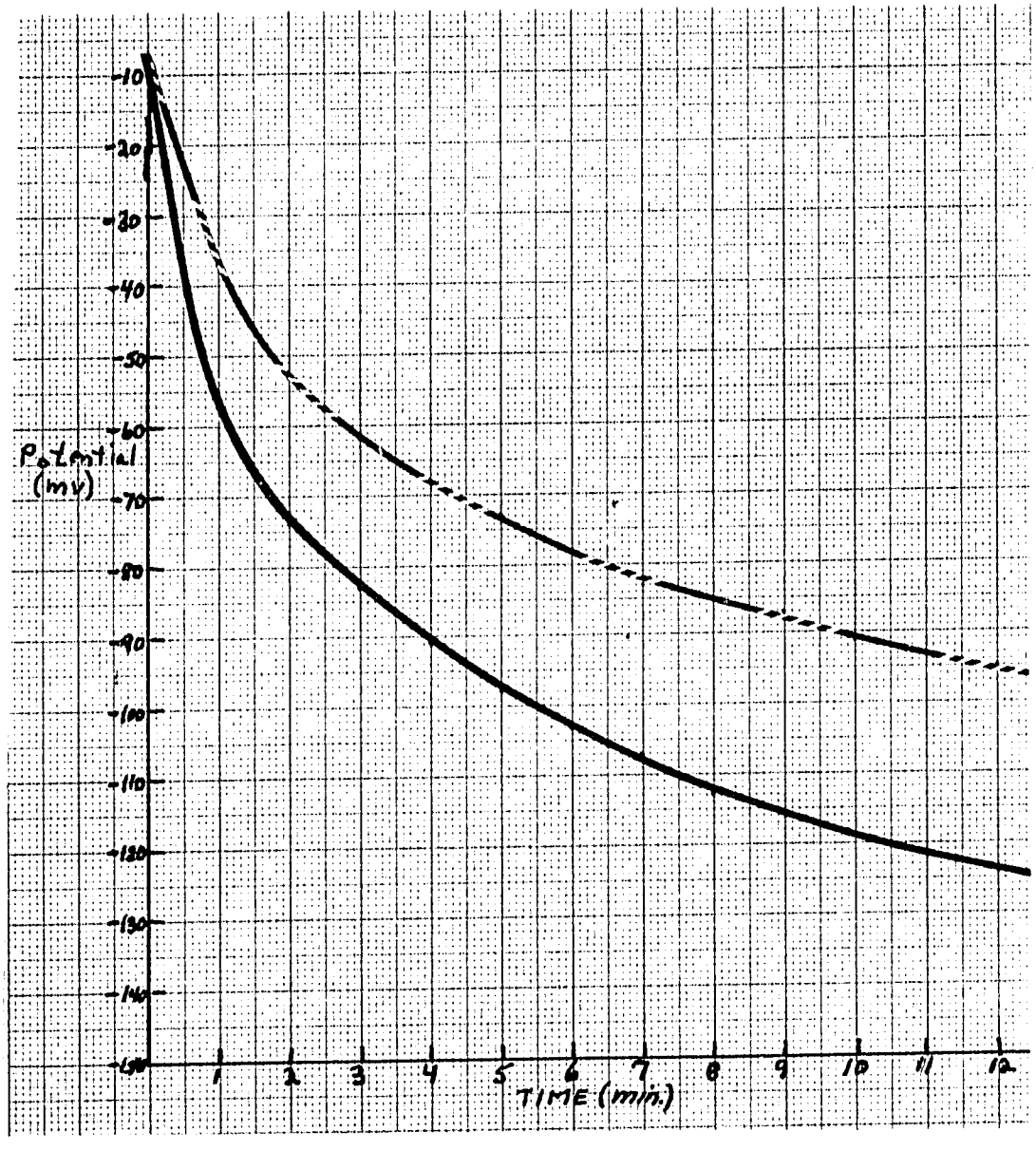

Fig. 5.--Potential change for solutions of equal concentration.

The potential growth curve cannot be described by a logarithmic relationship but can be dissected into two logarithmic growth curves. One of these corresponds to the slow growth portion of the curve, the second to the rapid growth portion. To accomplish this separation a plot is first made of the log of the voltage versus time. The linear portion of this curve is extrapolated to zero. The log of the difference between the extrapolated line and the experimental line is then plotted against time. Figure 6 shows the extrapolated line and Figure 7, the difference line for curve I. The slopes of the lines from curves I, II, and III are given in Table 2.

The phenomenon described above cannot be explained by means of a photoejection of an electron. Under the conditions of the experiment the only reaction that would occur would be the photohydrolysis of the complex. A possible explanation for the potential is that products or intermediates are formed whose redox potentials differ from the starting material. Therefore, the reaction was studied polarographically.

Polarographic Study

Initial results. The solution of $K_4Mo(CN)_8$ showed no anodic or cathodic waves between 0 and -1.8 volts before irradiation. During the course of irradiation, four waves were formed. Three of these were anodic and one cathodic

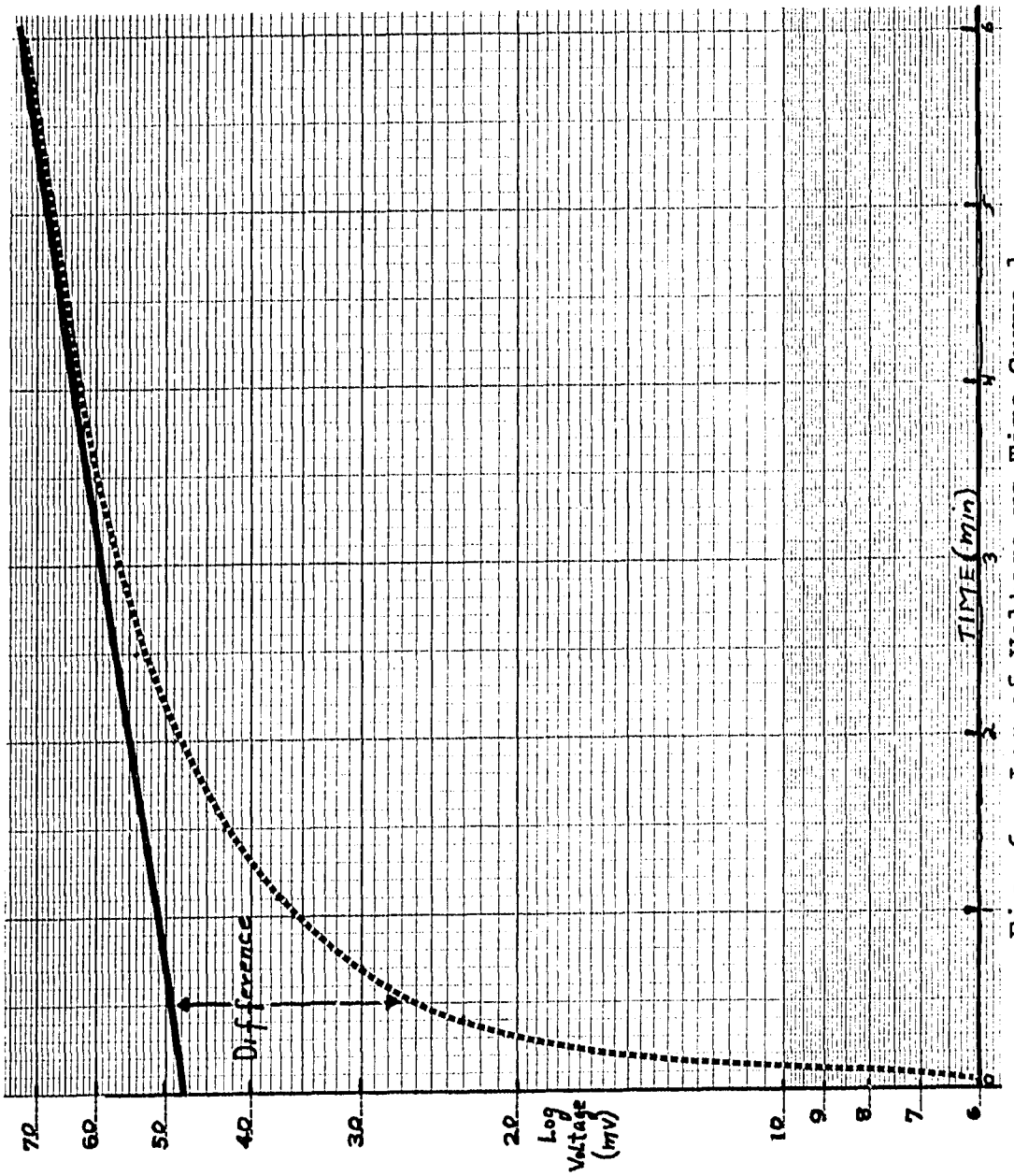

Fig. 6.--Log of Voltage vs Time Curve 1

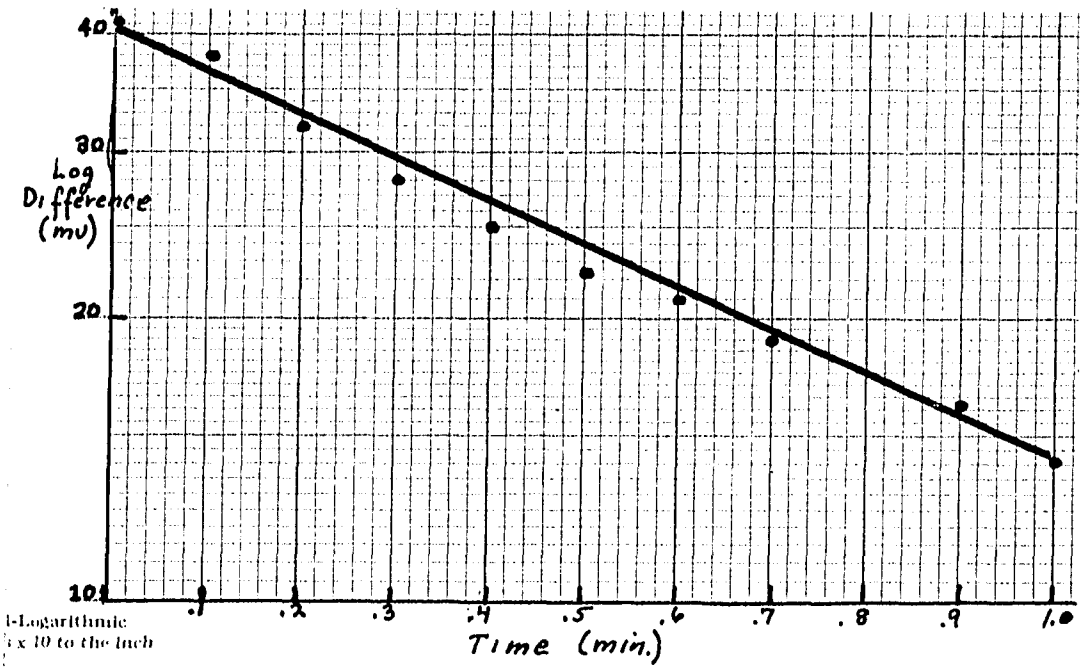

Fig. 7.--Log Difference vs Time

TABLE 2

SLOPES OF LOGARITHMIC POTENTIAL GROWTH CURVES

Curve	Difference Curve	Slow Growth Curve
I	2.8	.43
II	3.6	.44
III	5.5	.65

(Figure 8). The half wave potentials, $E_{1/2}$, for waves C and D were -1.1 and -1.6 volts, respectively. However, $E_{1/2}$ values for the cathodic wave and the first anodic wave, A and B, could not be determined since they represent the sum of an anodic and cathodic current. In effect, both an oxidation and a reduction occur simultaneously at the mercury electrode. Figure 9a shows what the two waves might look like if each were present alone. Figure 9b shows the change to the wave shape when both are present.

To insure that these waves were due to the photochemical reaction of the molybdate and not to a photochemical reaction of the molybdate with either the supporting electrolyte or mercury, several tests were performed.

(1) Irradiation of the supporting electrolyte alone and with added KCN showed that no polarographic waves were present other than the CN^- wave.

(2) Wave formation was seen in solutions of molybdate in two different supporting electrolytes, KCl and $KClO_3$.

(3) The four waves were still present when the solution without supporting electrolyte was irradiated outside the cell and then added to the supporting electrolyte.

When irradiation continued for a long period only waves A and D continued to increase in size while C and B

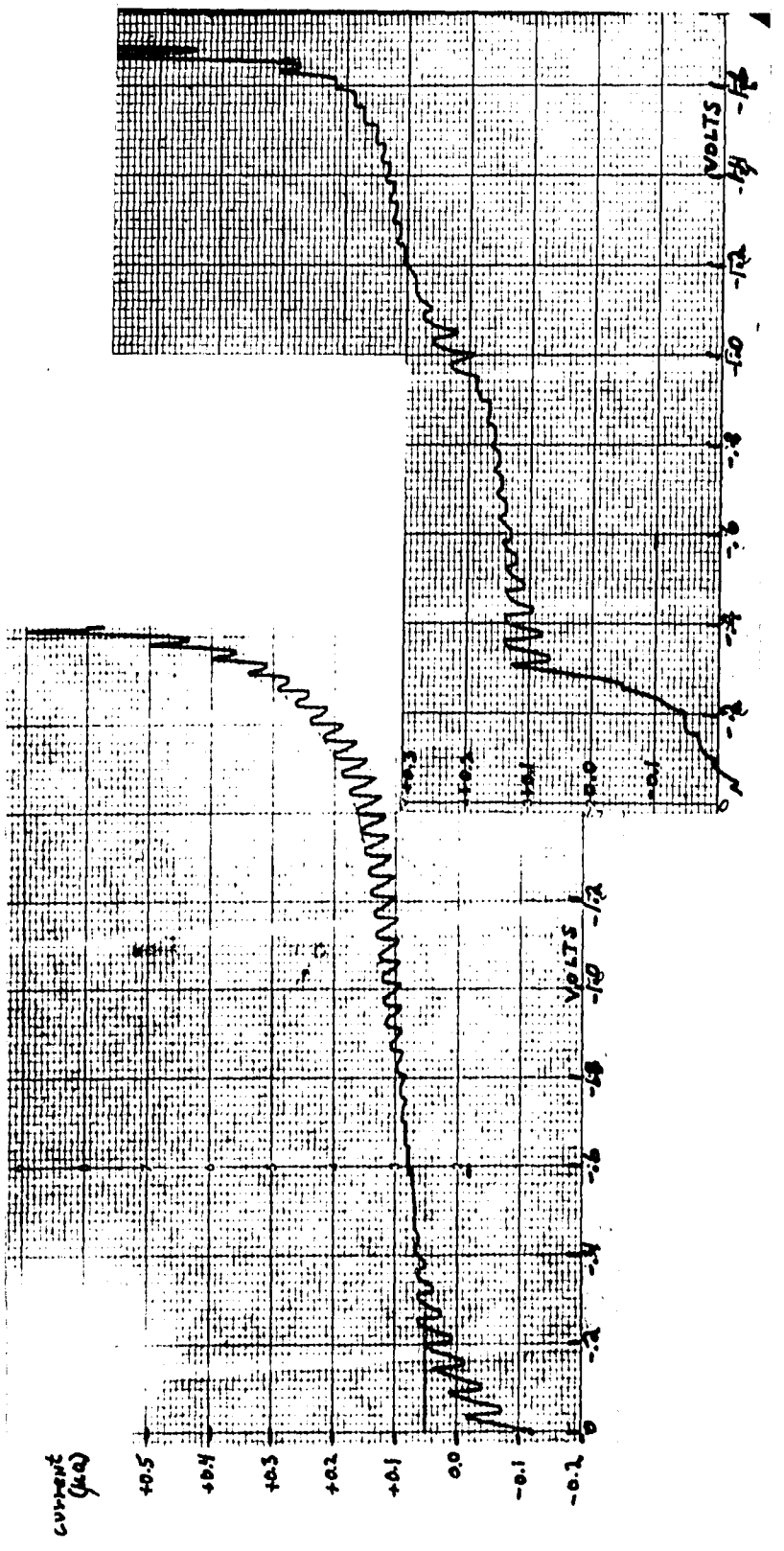

(a) before irradiation (b) during irradiation

Fig. 8--Polarogram of $Mo(CN)_8^{-4}$

(a) Polarograms if each were present alone

(b) Polarogram when both are present

Fig. 9.--Explanation of Wave Shape for Waves "A" and "B"

eventually disappeared. A had previously been identified as arising from the reaction of free cyanide with the mercury electrode

$$Hg + 2CN^- \rightarrow Hg(CN)_2 + 2e^-.$$

D was identified as the final product of the irradiation, $MoO_2(CN)_4^{-4}$, by matching half-wave potential and wave shapes in the two electrolytes.

Kinetic studies. Rate studies were made on waves A, B, and C to determine whether any kinetic relationship could be found between them. Scans were made from +0.5 volt to -1.5 volts at a rate of 100 seconds per scan. Wave height for B was determined by the current at -0.5 volt. The wave height for C was determined by the difference in current between -0.5 volts and -1.5 volts. Wave height for A was measured at +0.1 volt. During the total period of irradiation there was no nitrogen bubbling.

To allow for a slow growth of the intermediates, the low-intensity Xenon lamp was used. No attempt was made to make a quantitative judgment of rate; however, the growth curves for A, B, and C seem to be linear with time for the first 1000 seconds, indicating apparent zero-order kinetics. The rate of growth for C was slightly greater than that for B, while the growth of the cyanide wave, A, seems to be equal to the sum of the wave heights of B and C (Figure 10).

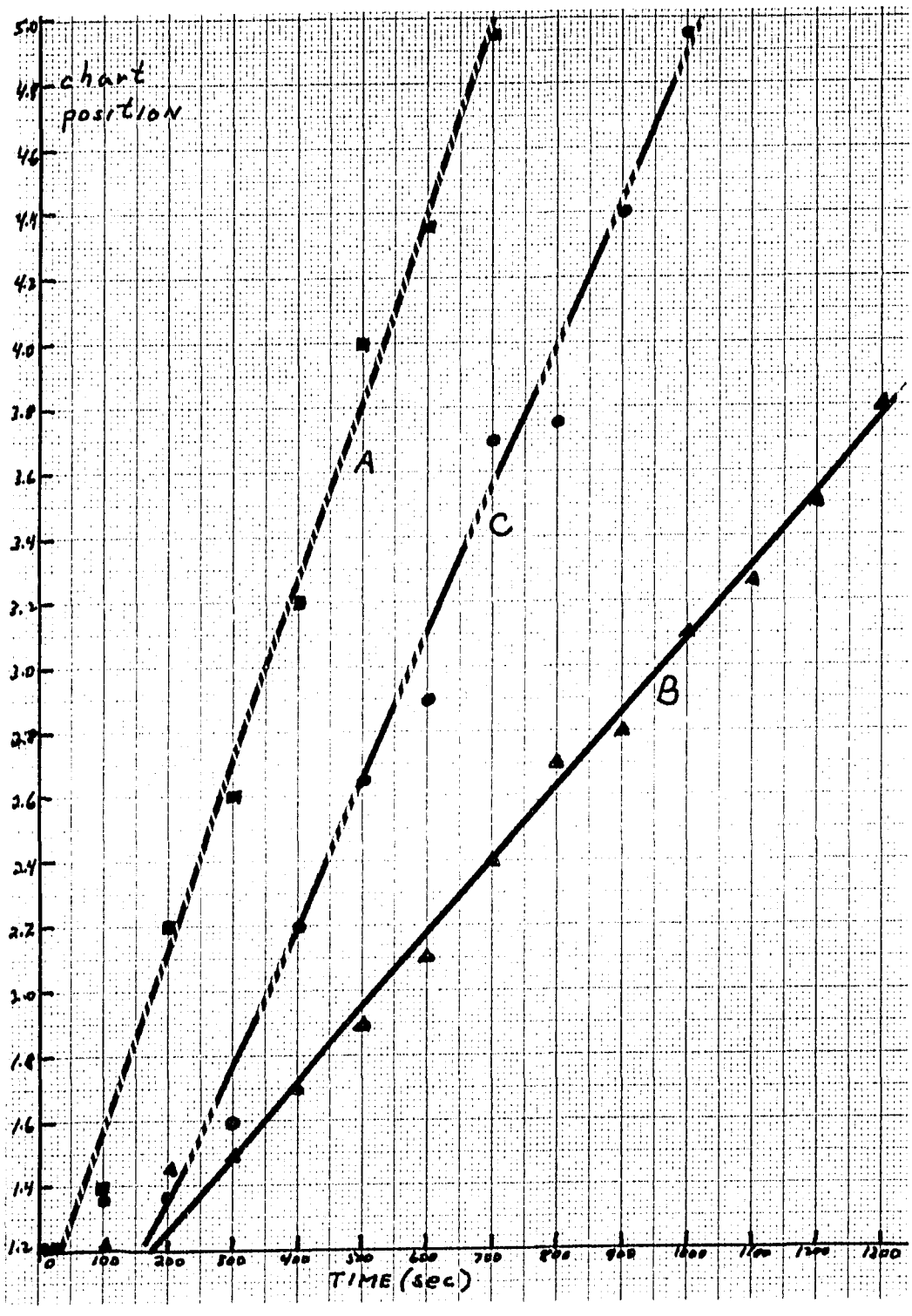

Fig. 10.--Growth of Waves "A" and "B" and "C"

If irradiation is terminated during the initial period of irradiation all three waves begin to decrease in size. This decay pattern is shown in Figure 11 for waves B and C. A linear relationship for this decay can be found if the reciprocal of the wave height is plotted versus time (Figure 12). This would indicate that an apparent second-order process is occurring for these two intermediates.

When the medium-pressure mercury lamp was used, the rate of reaction was considerably faster and both the formation and decay of the intermediates could be followed. Figure 13 shows the polarogram versus time for wave B. Figure 14 shows the pattern for waves B and C. A linear relationship can be found if a mechanism involving a second-order rate process is considered. Figure 15 is a plot of log B/C versus time. This apparent second-order relationship exists until B is completely reacted.

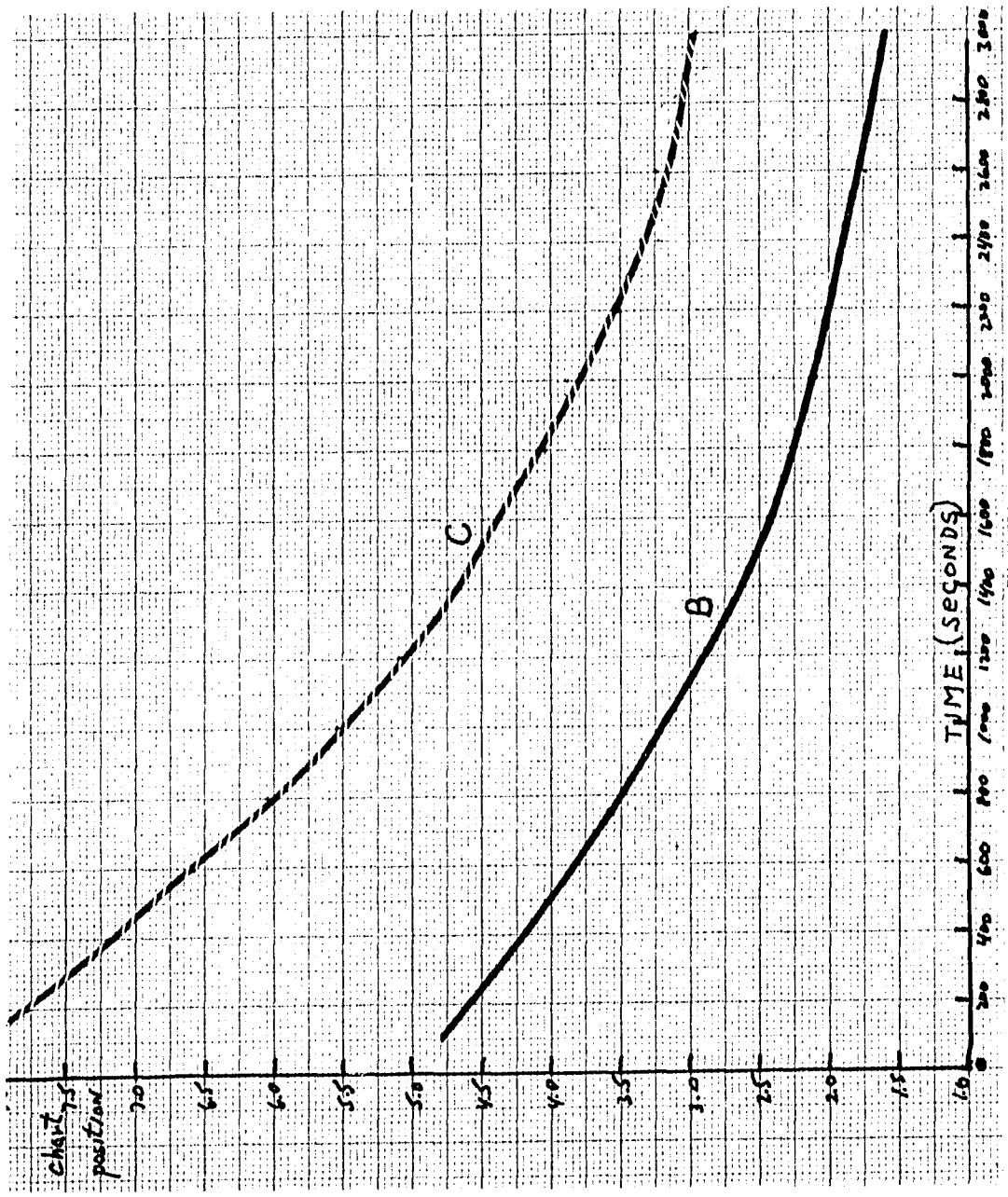

Fig. 11.--Dark Reaction Decay for Intermediates "B" and "C"

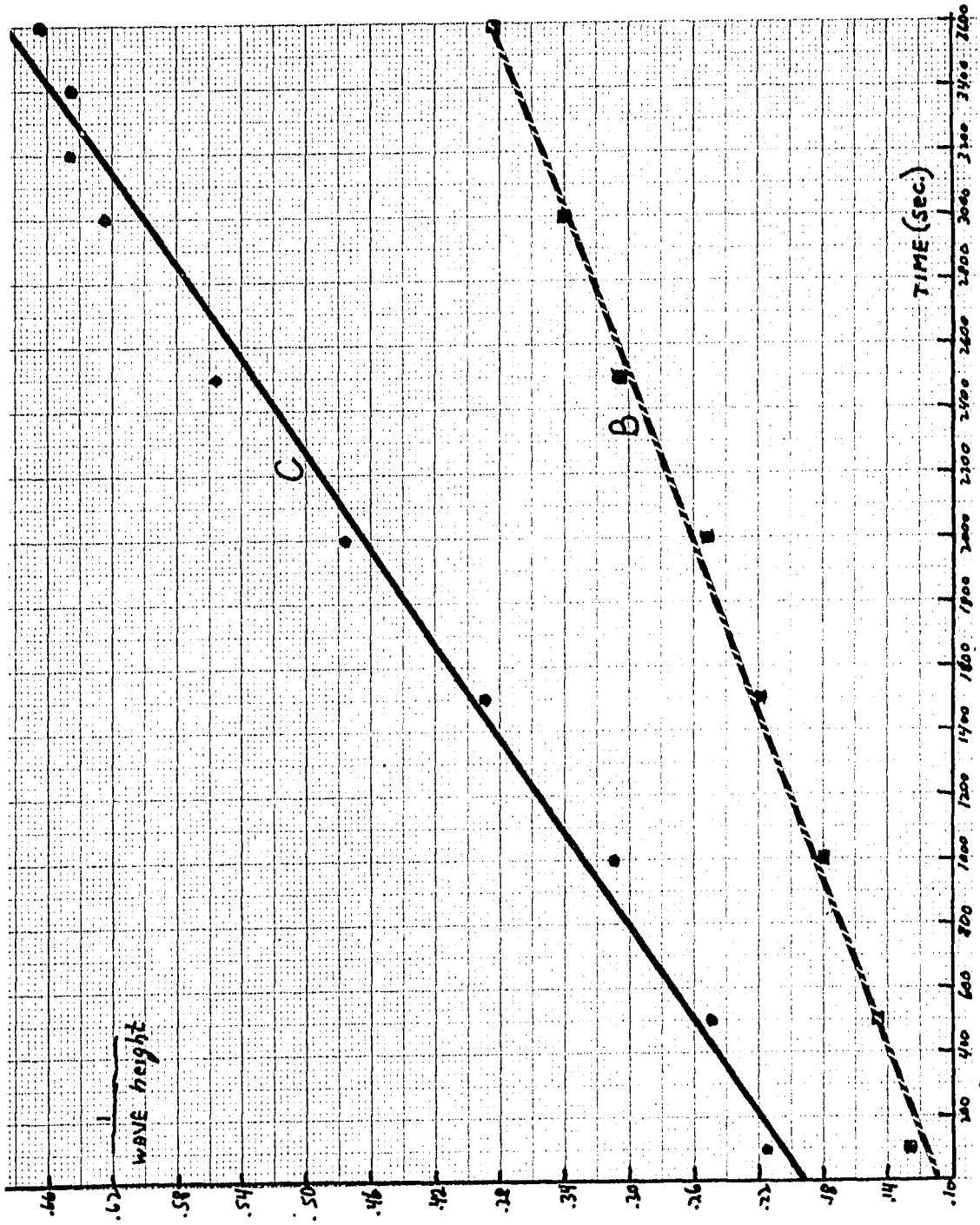

Fig. 12.--Apparent Second Order Decay for Waves "B" and "C"

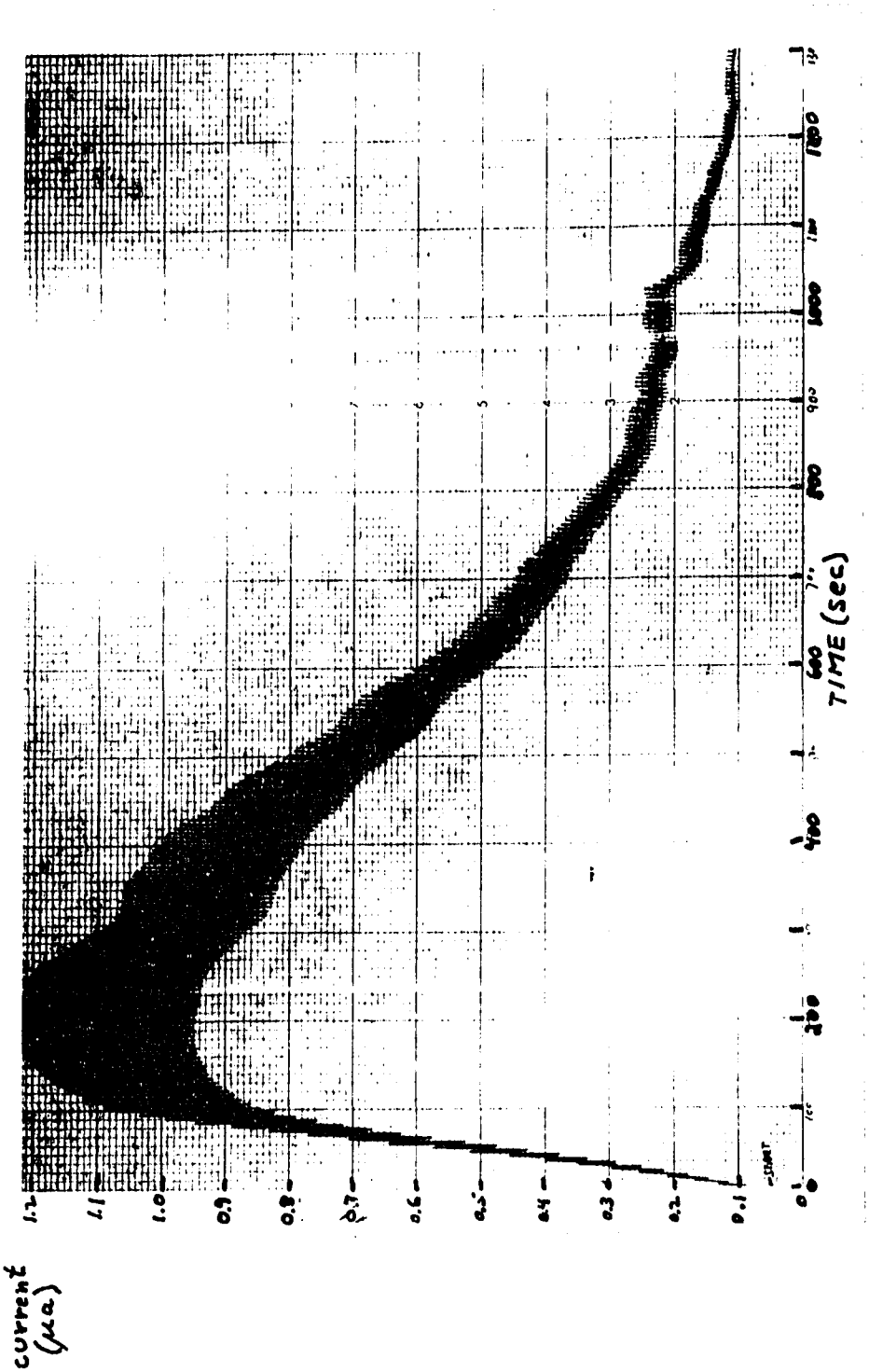

Fig. 13.--Polarogram for Growth of "B" with Time

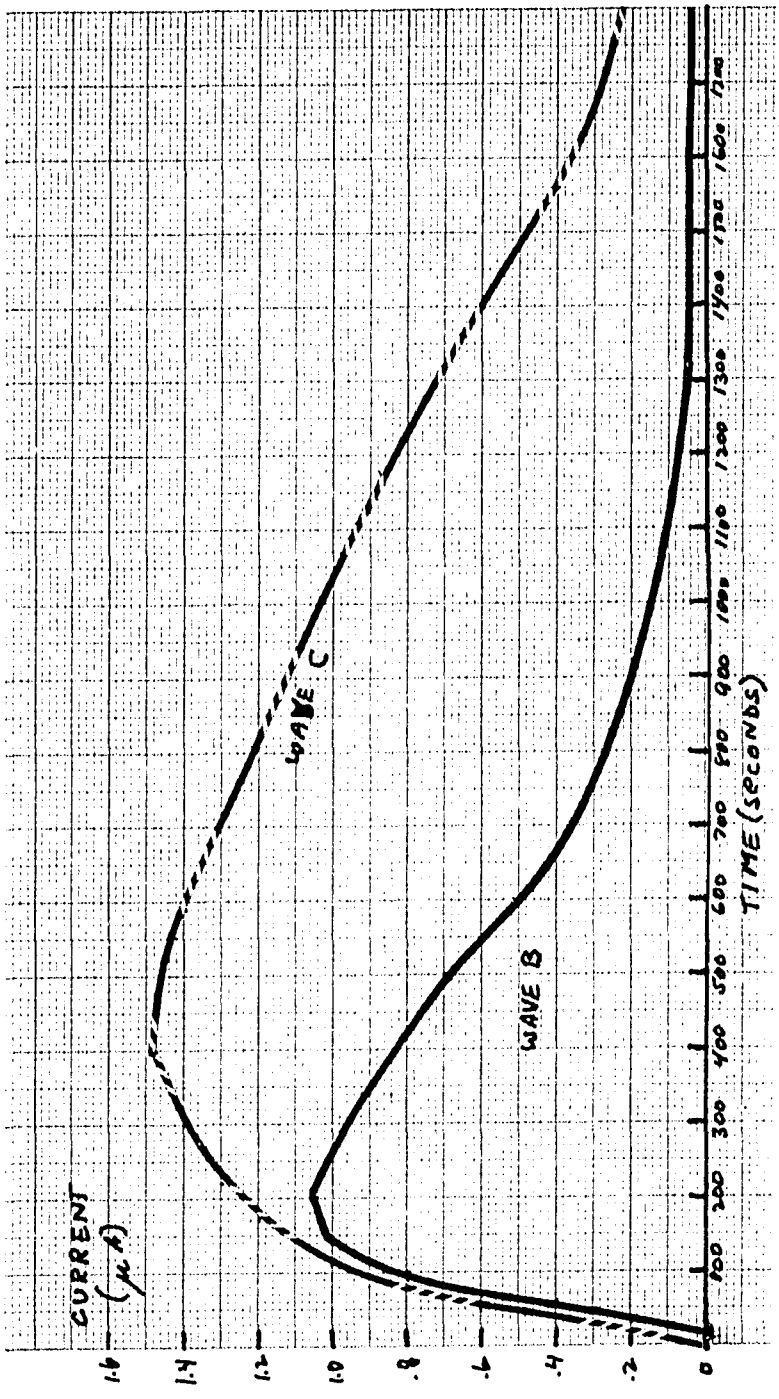

Fig. 14.--Photochemical Growth and Decay of Waves "B" and "C"

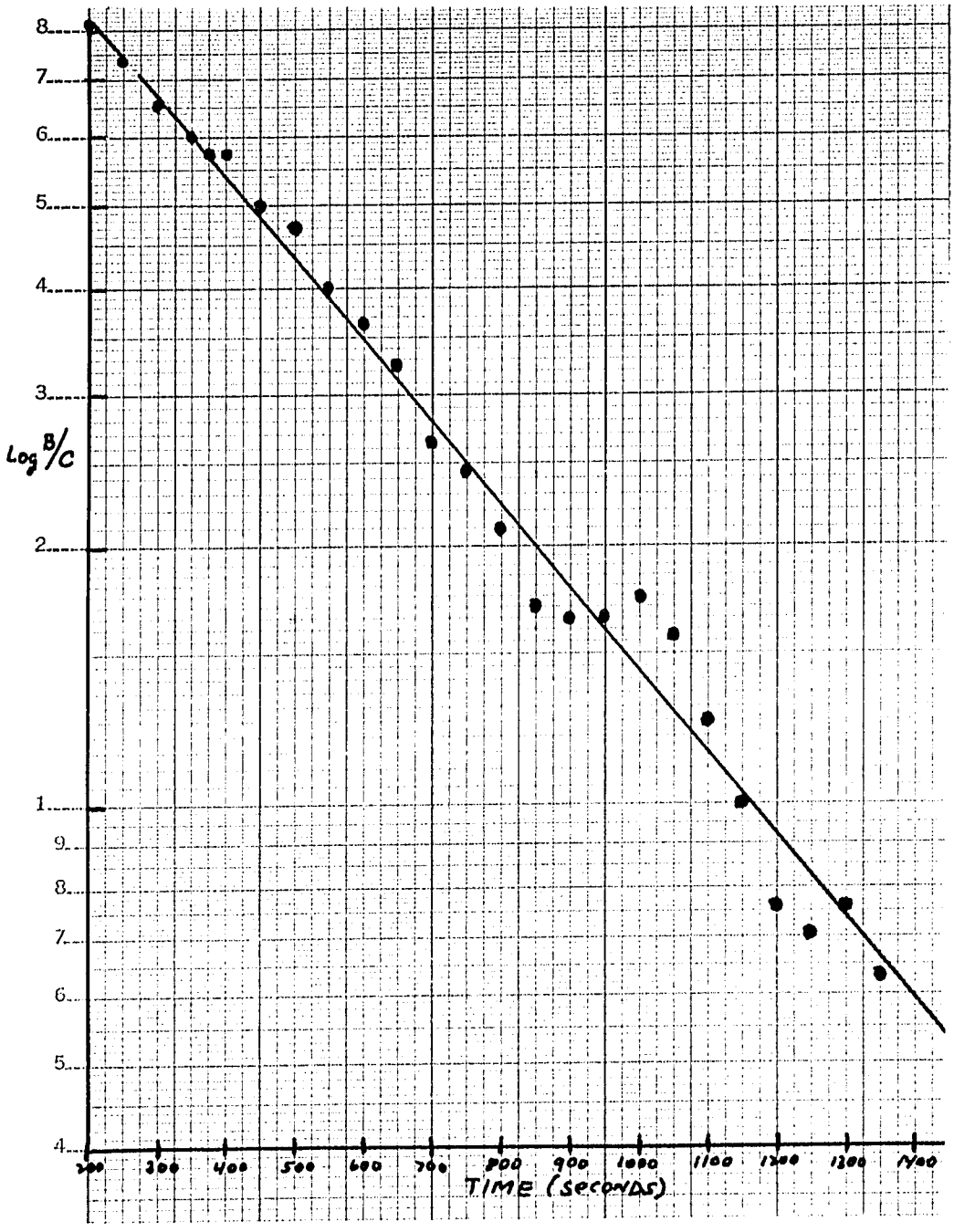

Fig. 15.--Second-Order Plot for Photochemical Decay of "B" and "C".

CHAPTER IV

DISCUSSION

Under the conditions that the photovoltaic effect was measured there can be no possibility that the voltage arises from photoejection of an electron from $Mo(CN)_8^{4-}$. There is, therefore, no primary change in the oxidation state of the molybdenum and other possible causes for the voltage must be found. Two factors in this system might be responsible for the voltage. The first of these is the decrease in the octacyanomolybdate concentration due to reaction. The effect of this would be similar to that of a concentration cell. The second is the differing oxidation potentials of possible intermediates or products of the reaction. This possibility is further strengthened by the results of the polarographic study. Both factors could be operating simultaneously and could in fact explain why the voltage versus time curve (Fig. 4) can be broken into two separate logarithmic relationships (Fig. 6 & 7).

The kinetic study indicates that the cyanide ion and intermediates B and C are formed in the primary step of the reaction.[16,18] Since the cyanide concentration is equal to the sum of the concentrations of B and C at any time, the formation of both must involve the loss of cyanide. Two of

the possible mechanisms are the following. The first is a one-photon process shown in equation 1.

$$(1) \quad Mo(CN)_8^{4-} \xrightarrow{h\nu} B + C + CN^-$$

The second is two one-photon processes involving simultaneous formation of B and C and is shown in equations 2 and 3.

$$(2) \quad Mo(CN)_8^{4-} \xrightarrow{h\nu} B + CN^-$$

$$(3) \quad Mo(CN)_8^{4-} \xrightarrow{h\nu} C + CN^-$$

The distinction between these two mechanisms is due to differences in photophysical rather than photochemical processes. Figure 16a shows the possible steps involved in mechanism 1. Light is absorbed by the molecule, exciting it to a high-energy state X. From this state a competition exists between reaction and radiationless decay to a lower state Y. A similar competition occurs from this state for either reaction or decay to the ground state. The products formed from states X and Y may be different. In Figure 16b, the second mechanism is shown. In this process, two photons of different energy are absorbed, one exciting the molecule to state X and the other to state Y, where two different reactions can occur.

The kinetic plot for the dark reaction seems to show that both B and C decay by a bimolecular mechanism. This

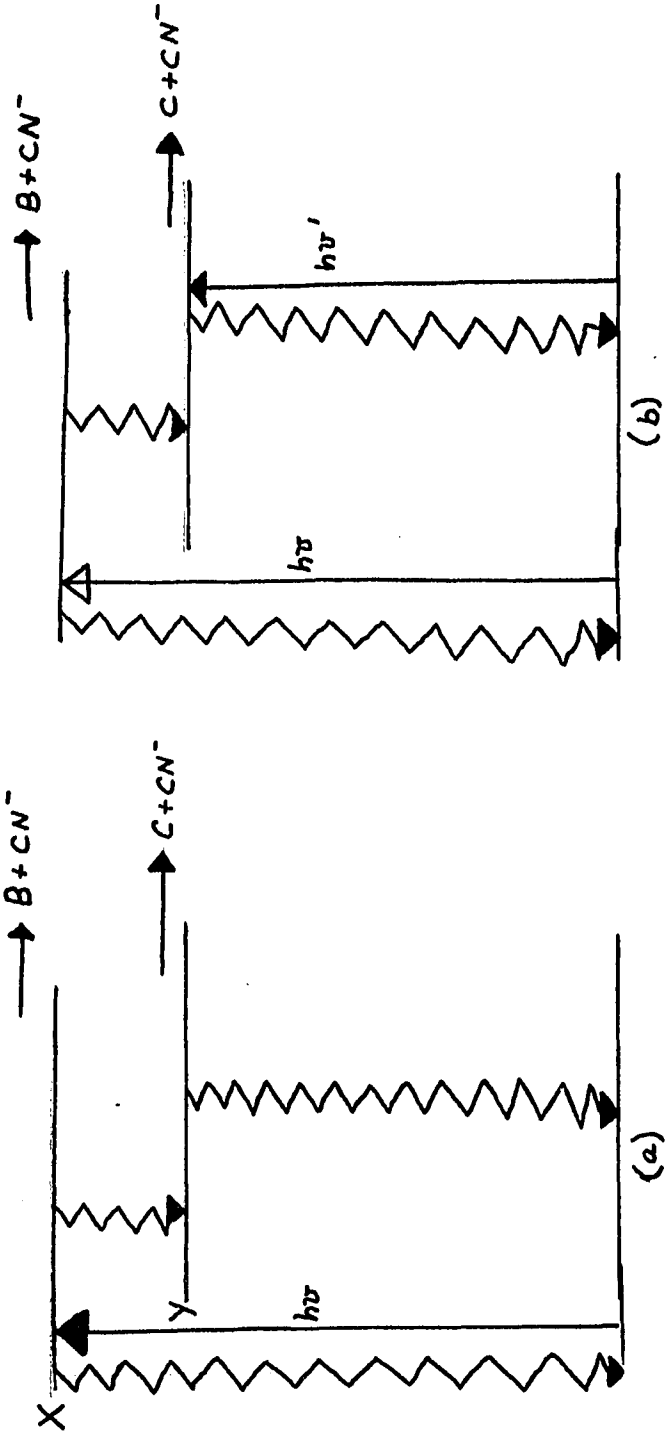

Fig. 16.--Photophysical Pathways

is in contradiction to previous evidence which indicated that the dark reaction is the reverse of the initial photochemical reaction and involves the reaction of cyanide ion with the substrate[15,16,18]. This contradiction can be more readily explained as an anomaly produced by the data rather than a new mechanism for decay. Further experimentation would be necessary to determine the kinetic relationship between the cyanide and the other substrates.

The second photochemical reaction occurs between the two intermediates, B and C. The kinetic plot shows the reaction to be bimolecular but a question still exists as to whether the product of this reaction is the final product of the reaction, equation 4, another intermediate, equation 5, or a possible side product, equation 6.

(4) $B + C \rightarrow D$

(5) $B + C \rightarrow$ intermediate $\rightarrow D$

(6) $B + C \rightarrow$ side product

Previous studies on the octacyanomolybdate (IV) ion have indicated that the pathway from the intermediate to the final product is not known but that it may involve the absorption of at least one more photon of light[20]. In all of these studies, the formation of only one of the possible intermediate, $Mo(CN)_7^{3-}$, has been seen[17]. It is possible, however, that two intermediates are formed of such

similar properties that they could not be distinguished by normal absorption techniques. This may be the case with two isomers of $Mo(CN)_7^{3-}$. One isomer would be formed from the loss of a cyanide from a relatively stable position and the other from a less stable position. This would explain the reaction from two different excited states of the molecule, one higher in energy than the other.

Once these two isomers are formed it is possible for one or both to absorb a second photon. Three possible pathways for the excited molecule are shown in equations 7 through 9.

(7) $Mo(CN)_7^{3-} \xrightarrow{h\nu} \sim\!\!\rightarrow MoO_2(CN)_4^{4-}$

(8) $2\ Mo(CN)_7^{3-} \xrightarrow{h\nu} Mo(CN)_6^{2-} + Mo(CN)_8^{4-}$

$\downarrow$

$MoO_2(CN)_4^{4-}$

(9) $2Mo(CN)_7^{3-} \xrightarrow{h\nu} (Mo(CN)_7)_2^{6-}$

Equation 7 shows a monomolecular loss of another cyanide leading eventually to the final product. Equation 8 involves transfer of a cyanide and equation 9 involves the formation of a polymeric final product.

In conclusion, it should be emphasized that the polarographic study of a photochemical reaction exhibits

certain strengths and weaknesses. Its basic strength is its ability to distinguish intermediates in a reaction which might otherwise not be observed. Its basic weakness is its inability to follow fast reaction kinetics.

BIBLIOGRAPHY--PART II

1. M. Navidi, H. Brittain, A. Heller, Science, 169, 980 (1970).

2. V. Balzini, V. Carassiti, "Photochemistry of Coordination Compounds," Academic Press, New York, N.Y., p. 123 (1970).

3. P. Airey, F. Dainton, Proc. Royal Soc. (London), A291, 340 (1966).

4. (a) S. Ohno, Bulletin of the Chem. Soc. of Japan, 40, 1770 (1967).
(b) S. Ohno, Bulletin of the Chem. Soc. of Japan, 40, 1776 (1967).
(c) S. Ohno, Bulletin of the Chem. Soc. of Japan, 40, 1779 (1967).

5. M. Shirom, G. Stein, J. Chem. Phys., 55, 3372 (1971).

6. W. Waltz, A. Adamson, P. Fleishauer, J. Amer. Chem. Soc., 89, 3923 (1967)

7. W. Waltz, A. Adamson, J. Phys. Chem., 73, 4250 (1969).

8. A. Bettelheim, M. Shirom, Chem. Physics Letters, 9, 166 (1971).

9. B. Baron, P. Chartier, P. Delahay, R. Lugo, J. Chem. Phys., 51, 2562 (1969).

10. P. Delahay, P. Chartier, L. Nemec, J. Chem. Phys., 53, 3126 (1970).

11. S. Cotton, G. Wilkinson, "Advanced Inorganic Chemistry," Wiley-Interscience N.Y., pp. 969, 970 (1970).

12. J. Perumareddi, A. Liehr, A. Adamson, J. Amer. Chem. Soc., 85, 249 (1963).

13. A. Adamson, J. Walker, M. Volpe, J. Amer. Chem. Soc., 72, 4030 (1950).

14. A. Adamson, A. Sporer, J. Amer. Chem. Soc., 80, 3865 (1958).

15. S. Asperger, I. Murati, D. Pavlonic, J. Chem. Soc., 730 (1960).

16. A. Adamson, J. Perumareddi, Inorg. Chem., 4, 247 (1965).

17. R. Mitra, B. Sharma, H. Mohan, Can. J. Chem., 47, 2317 (1969).

18. R. Mitra, B. Sharma, H. Mohan, Indian J. Chem., 7, 1162 (1969).

19. (a) J. Van de Poel, H. Neumann, Inorg. Chem., 7, 2086 (1968).

(b) S. Lippard, B. Russ, Inorg. Chem., 6, 1943 (1967).
(c) S. Lippard, H. Nozaki, B. Russ, Chem. Comm., 118 (1967).

20. D. Drum, Ph.D. Dissertation, Univ. of Mass., 1971, p. 88. Dissertation # 71-23,034.

21. W. Palmer, "Experimental Inorganic Chemistry," Cambridge Univ. Press, 1959, pp. 410-414.

22. G. Schlessinger, "Inorganic Laboratory Publications," N.Y., 1962, pp. 91-94.